NEUROSCIENCE

Long noncoding RNA Gm2694 drives depressive-like behaviors in male mice by interacting with GRP78 to disrupt endoplasmic reticulum homeostasis

Hong-Sheng Chen[1,2,3]†, Ji Wang[1]†, Hou-Hong Li[1]†, Xiao Wang[1], Shao-Qi Zhang[1], Tan Deng[1], Yu-Ke Li[1], Ruo-Si Zou[1], Hua-Jie Wang[1], Rui Zhu[1], Wen-Long Xie[1], Gang Zhao[4]*, Fang Wang[1,2,3,5,6]*, Jian-Guo Chen[1,2,3,5,6]*

Long noncoding RNAs (lncRNAs) are involved in various biological processes and implicated in the regulation of neuronal activity, but the potential role of lncRNAs in depression remains largely unknown. Here, we identified that lncRNA Gm2694 was increased in the medial prefrontal cortex (mPFC) of male mice subjected to chronic social defeat stress (CSDS). The down-regulation of Gm2694 in the mPFC alleviated CSDS-induced depressive-like behaviors through enhanced excitatory synaptic transmission. Furthermore, we found that Gm2694 preferentially interacted with the carboxyl-terminal domain of 78-kilodalton glucose-regulated protein (GRP78), which abrogated GRP78 function and disrupted endoplasmic reticulum homeostasis, resulting in a reduction of the surface expression of AMPA receptors (AMPARs). Overexpression of GRP78 in the mPFC promoted the surface expression of AMPARs and attenuated the CSDS-induced depressive-like behaviors of mice. Together, our results unraveled a previously unknown role of Gm2694 in regulating endoplasmic reticulum homeostasis and excitatory synaptic transmission in depression.

INTRODUCTION

Depression is a common illness worldwide, with an estimated 5% of adults affected, and approximately 280 million people in the world have depression (*1*, *2*). Because of either side effects or lack of effectiveness, antidepressant treatment produces unsatisfactory results. Functional and structural abnormalities of prefrontal cortex (PFC) have been reported in both individuals with current major depressive disorder (MDD) and those at increased vulnerability to MDD (*3*), which are consistent with the studies of the postmortem human brain, that decreased expression of synapse-related genes and loss of synapses are observed in the PFC of patients with depression (*4*, *5*). Understanding the molecular underpinnings leading to synaptic dysfunction will aid in the development of therapy for depression.

Long noncoding RNAs (lncRNAs) are transcripts longer than 200 nucleotides that lack protein-coding function (*6*). They have been recognized to be involved in several biological processes by interacting with DNA, RNA, or protein through distinct modes of action. For example, lncRNAs act as decoys to titrate away RNA binding proteins. In addition, lncRNAs function as molecular signals in response to unique stimuli, altering the stability and translation of cytoplasmic mRNAs, and interfere with signaling pathways. lncRNAs serve as guides to recruit chromatin-modifying enzymes in cis or in trans to target genes (*7*). Accumulating evidence demonstrates that lncRNAs play an important role in regulating synaptic morphology and function (*8*, *9*). For example, Malat1, an abundant lncRNA that localizes to the nuclear speckles, modulates synapse formation by regulating the expression of genes involved in synaptogenesis (*10*). The mutation of *PTCHD1-AS* exon 3 impairs excitatory synaptic transmission in gene-edited induced pluripotent stem cell–derived neurons (*11*). The expression of lncRNA GM12371 is up-regulated by adenosine 3′,5′-monophosphate signaling and is necessary for synaptic transmission (*12*). In addition, several lncRNAs are more likely to be misregulated in neurological disorders including autism (*11*, *13*), Angelman syndrome (*14*), Alzheimer's disease (*15*), cocaine addiction (*16*), schizophrenia (*17*), and depression (*18*). For instance, lncRNA LINC00473 is a female-specific driver of stress resilience that is aberrant in female depression (*19*). Nevertheless, the role of lncRNAs in depression remains to be further determined.

Several lines of evidence have demonstrated that chronic stress attenuates AMPA receptor (AMPAR)–mediated synaptic transmission (*20*–*22*). AMPARs are tetrameric ion channels that are assembled into functional receptors in the endoplasmic reticulum (ER) by ER-resident interactors (*23*). One mechanism that regulates the quality control of AMPARs, export from the ER, is the unfolded protein response (UPR) (*24*). UPR is a transcriptional and translational response to the accumulation of unfolded proteins in the ER. When unfolded proteins accumulate in the ER, UPR is activated and works to balance the load on the molecules in charge of folding the proteins by lowering the number of unfolded proteins present in the cell. However, during prolonged or overwhelming ER stress, UPR fails to restore ER homoeostasis and results in an activation of apoptotic cascade (*25*). There are three ER-resident transmembrane proteins orchestrating the UPR: the inositol-requiring enzyme 1 (IRE1), the protein kinase-like ER kinase (PERK), and the activating transcription factor 6 (ATF6). The 78-kDa glucose-regulated protein (GRP78), also called binding immunoglobulin protein, is a central

[1]Department of Pharmacology, School of Basic Medicine, Tongji Medical College, Huazhong University of Science and Technology, 430030 Wuhan, China. [2]The Research Center for Depression, Tongji Medical College, Huazhong University of Science, 430030 Wuhan, China. [3]The Key Laboratory for Drug Target Researches and Pharmacodynamic Evaluation of Hubei Province, 430030 Wuhan, China. [4]Department of Emergency Surgery, Union Hospital, Tongji Medical College, Huazhong University of Science and Technology, 430022 Wuhan, China. [5]The Key Laboratory of Neurological Diseases (HUST), Ministry of Education of China, 430030 Wuhan, China. [6]Laboratory of Neuropsychiatric Diseases, The Institute of Brain Research, Huazhong University of Science and Technology, 430030 Wuhan, China.
*Corresponding author. Email: chenj@mails.tjmu.edu.cn (J.G.C.); wangfanghust@hust.edu.cn (F.W.); gangzhao@hust.edu.cn (G.Z.)
†These authors contributed equally to this work.

regulator for ER stress due to its role as a major ER chaperone. Under physiological condition, GRP78 interacts with ER-luminal sensor domains of the three UPR-transducer proteins IRE1, PERK, and ATF6, which are located in ER membranes to inactivate the UPR and maintain ER homeostasis. Once ER stress occurs, unfolded/misfolded proteins are predominantly accumulated in the ER lumen, which compete with GRP78 binding to the UPR sensor proteins, and let the fact that GRP78 is released from the sensor proteins. This leads to the activation of downstream signaling of these three UPR effector proteins and increases the expression of GRP78 protein in the ER lumen (*26*).

GRP78 is a chaperone protein localized primarily in the ER lumen, where it assists in proper protein folding by facilitating assembly and trafficking of misfolded proteins. For example, GRP78 selectively interacts with the N-terminal domain of GluN2A subunit of *N*-methyl-D-aspartate receptor (NMDAR) and participates in the synaptic insertion of GluN2A-containing NMDAR (*27*). In addition, GRP78 is reported to recognize and bind to GluA1 and GluA2 subunits of AMPAR (*28*–*30*), indicating a key role of GRP78 in the trafficking and postsynaptic localization of AMPAR. Several studies have shown that the expression of GRP78 is increased in the temporal cortex (*31*) and PFC (*32*) of individuals with MDD.

lncRNAs have been demonstrated to be associated with ER stress response (*33*, *34*); however, whether synaptic transmission is altered by lncRNA-regulated ER homeostasis is largely unknown. Here, by using lncRNA microarray profiling and viral-mediated molecular manipulation, we found that lncRNA Gm2694 impaired excitatory synaptic transmission and contributed to depressive-like behaviors in male mice. Activation of lncRNA Gm2694 disrupted ER homeostasis via interacting with C-terminal domain of GRP78, leading to the decrease in surface expression of AMPARs.

RESULTS

lncRNA Gm2694 is up-regulated by chronic stress in the mPFC of male mice

To investigate the potential role of lncRNAs in depression, chronic social defeat stress (CSDS), we used an extensively used animal model of depression and assessed the depressive-like behaviors by social interaction test (SIT) and sucrose preference test (SPT) (Fig. 1A) (*35*). Compared with control and resilient mice, susceptible mice spent less time engaging in social interaction and displayed reduced social interaction ratio (Fig. 1, B to D) and sucrose preference (Fig. 1E). Then, an established lncRNA microarray analysis was applied in RNAs that isolated from medial PFC (mPFC) of control and CSDS-treated (susceptible) mice. The differentially expressed lncRNAs were analyzed using a $\log_2$ fold change (FC) ≥ 2.0 and a $P \leq 0.01$. It was found that only 37 lncRNAs were up-regulated, and 50 lncRNAs were down-regulated in the mPFC of CSDS-treated mice (Fig. 1F and file S1), among which Gm2694, the lncRNA encoded by a gene at chromosome 8qc3, was identified as the most obviously up-regulated lncRNA in CSDS-treated mice (Fig. 1, F and G, and fig. S1, A and B). Since the functions of lncRNAs depend on their subcellular localization (*36*), fluorescence in situ hybridization (FISH) assays were performed to investigate the distribution of Gm2694 in HT22 cells. As shown in Fig. 1H, Gm2694 was mainly distributed in the cytoplasm, prompting that the cytoplasmic Gm2694 may be involved in its biological function. Although Gm2694 was expressed throughout the body (fig. S1C), the level of Gm2694 was increased in the mPFC of CSDS-treated mice (Fig. 1I) but remained unchanged in anterior cingulate cortex, nucleus accumbens, dorsal hippocampus, basolateral amygdala, and cerebellum (fig. S1, D to H). There was a negative correlation between the level of Gm2694 and social interaction ratio (Fig. 1J). By using the cytoplasmic and nuclear RNA purification kit, it was shown that the level of Gm2694 was increased in the cytoplasm of mPFC from depressed mice (Fig. 1K). Next, we used the primary culture of cortical neurons and glia cells to investigate which cell type Gm2694 was expressed in. The results showed that Gm2694 was expressed in neurons, microglia, and astrocytes (fig. S2A) and located in the ER and Golgi apparatus of neurons (fig. S2B). These results indicate that chronic stress increases the expression of Gm2694 in the mPFC of CSDS-treated mice.

Knockdown of Gm2694 in the mPFC prevents CSDS-induced depressive-like behaviors via enhancing excitatory synaptic transmission

To determine the impact of Gm2694 in the depressive-like behaviors, we constructed an effective short hairpin RNA (shRNA) for the specific knockdown of Gm2694 with lentivirus (LV-sh*Gm2694*), which was microinjected into the mPFC to decrease Gm2694 expression (Fig. 2A and fig. S3, A and B). Knockdown of Gm2694 improved the depressive-like behaviors of defeated mice, as shown by reduced social avoidance (Fig. 2, B to D) and increased sucrose preference (Fig. 2E), but not in control mice (fig. S3, C to E).

Considering that accumulating evidence demonstrates aberrant glutamatergic function in depression (*20*, *37*) and a previous study in our laboratory showed that chronic stress reduced glutamate receptor–mediated synaptic transmission by increasing microRNA-214-3p in the mPFC of depressed mice (*35*), we wondered whether the antidepressant action of Gm2694 was involved in the regulation of glutamatergic neurotransmission. Western blotting analysis showed that the surface expressions of GluA1 and GluA2 subunits of AMPAR were markedly decreased in the mPFC of CSDS-treated mice but reversed by application of LV-sh*Gm2694* into the mPFC. On the contrary, the total levels of GluA1 or GluA2 were unchanged by CSDS or LV-sh*Gm2694* injection (Fig. 2, F and G).

Next, whole-cell patch-clamp recording was used to further investigate the effect of Gm2694 on excitatory synaptic transmission of pyramidal neurons in mPFC slices. AMPAR-mediated miniature excitatory postsynaptic currents (mEPSCs) were recorded in the presence of tetrodotoxin (a selective sodium channel blocker; 10 μM), (2R)-amino-5-phosphonovaleric acid (AP5) (an NMDAR antagonist; 50 μM), and bicuculline (a γ-aminobutyric acid type A receptor antagonist; 20 μM). Consistent with our previous studies (*35*), both amplitude and frequency of AMPAR-mediated mEPSCs were reduced in the mPFC of CSDS-treated mice compared with that of control mice, which were reversed by application of LV-sh*Gm2694* into the mPFC (Fig. 2, H to L). However, LV-sh*Gm2694* failed to affect AMPAR-mediated mEPSCs of control mice (fig. S4, A to E). There were no notable changes in the decay time and rise time of mEPSCs in all cases (fig. S4, F and G), suggesting that LV-sh*Gm2694* does not alter the kinetics of excitatory synaptic currents in the mPFC. Next, the evoked AMPAR-mediated EPSCs (AMPAR-eEPSCs) were recorded in the mPFC of mice. It was found that application of LV-sh*Gm2694* into the mPFC reversed the decrease in the amplitude of the AMPAR-eEPSC in the mPFC of CSDS-treated mice (Fig. 2, M and N). In addition, the dendritic spine densities of

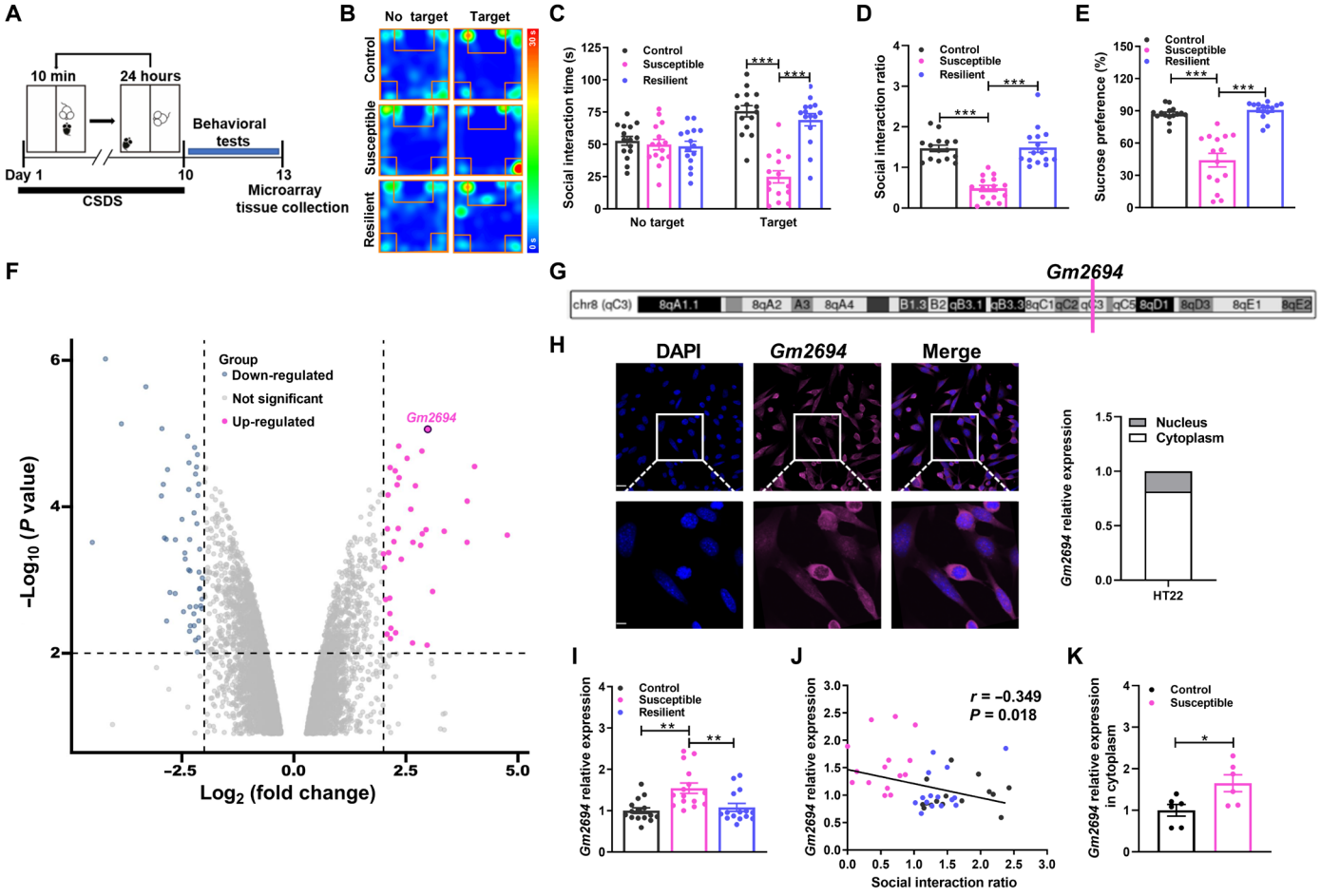

Fig. 1. The expression of lncRNA Gm2694 is up-regulated in the mPFC of susceptible mice. (**A**) The timeline of experimental procedure. (**B**) Heatmaps of time spent in the SIT. (**C**) Susceptible mice spent less time in the interaction zone when the target was present than control and resilient mice ($n = 15$ mice per group). (**D**) Susceptible mice had a significant lower interaction ratio than control and resilient mice ($n = 15$ mice per group). (**E**) Susceptible mice exhibited reduced sucrose preference ($n = 15$ mice per group). (**F**) Volcano plot showing the microarray analysis of differentially expressed lncRNAs in the mPFC between control and susceptible mice. (**G**) Chromosomal position of Gm2694 in University of California Santa Cruz (UCSC) database. (**H**) FISH results of the distribution of Gm2694 in HT22 cells (left). FISH statistical data of Gm2694 for subcellular localization (right). $n = 6$. Scale bars, 20 μm (top) and 5 μm (bottom). (**I**) The mRNA level of Gm26964 was increased in the mPFC of susceptible mice. Gm2694 levels were normalized to control mice ($n = 15$ mice per group). (**J**) Correlation between Gm2694 level in the mPFC and social interaction ratio in control and susceptible mice ($n = 15$ mice per group). (**K**) The mRNA level of Gm2694 was increased in cytoplasm of susceptible mice. Gm2694 levels were normalized to control mice ($n = 6$ mice per group). All data are presented as the means ± SEM, with each point representing data from an individual. $^*P < 0.05$, $^{**}P < 0.01$, and $^{***}P < 0.001$ by one-way analysis of variance (ANOVA) (C, D, E, and I) followed by Bonferroni's post hoc test or Pearson correlation test (J) or Student's *t* test (K). The statistical details can be found in table S1.

pyramidal neurons were measured in the mPFC of mice. Dendrites from stressed mice showed a decrease in spine density compared with that of control mice but were reversed by microinjection of LV-sh*Gm2694* into the mPFC (fig. S4, H and I). Together, these results suggest that the knockdown of Gm2694 in the mPFC alleviates CSDS-induced synaptic dysfunction and depression-like behaviors.

Overexpression of Gm2694 in the mPFC contributes to depressive-like behaviors

Given that the knockdown of Gm2694 in the mPFC ameliorated depressive-like behaviors, we asked whether the overexpression of Gm2694 in the mPFC contributed to depressive-like behaviors. Four weeks after microinjection of recombinant adeno-associated viral vectors encoding green fluorescent protein (AAV-GFP) or Gm2694 (AAV-Gm2694) into the mPFC, mice were performed behavioral tests and subsequently exposed to a microdefeat stress, which consisted of 5 min of physical aggression by an unfamiliar CD-1 mouse and was not sufficient to induce depressive-like behaviors in mice (*38*). Twenty-four hours after a microdefeat stress, mice were tested in the SIT and SPT (Fig. 3A). A representative section illustrating accurate bilateral microinjection into the mPFC can be seen in Fig. 3B. It was found that the expression of Gm2694 was increased in AAV-Gm2694–treated mice exposed to microdefeat stress compared with that of AAV-GFP–treated mice (Fig. 3C). In addition, AAV-Gm2694–treated mice exposed to microdefeat stress displayed a reduction in the time and the ratio of time spent in the interaction zone (Fig. 3, D to F), together with the decrease in sucrose preference (Fig. 3G) compared with that of AAV-GFP–treated mice.

Next, we measured AMPAR-mediated mEPSCs and observed that the amplitude and frequency were decreased in the AAV-Gm2694–treated mice exposed to microdefeat stress compared with that of AAV-GFP–treated mice (Fig. 3, H to L); however, decay time and

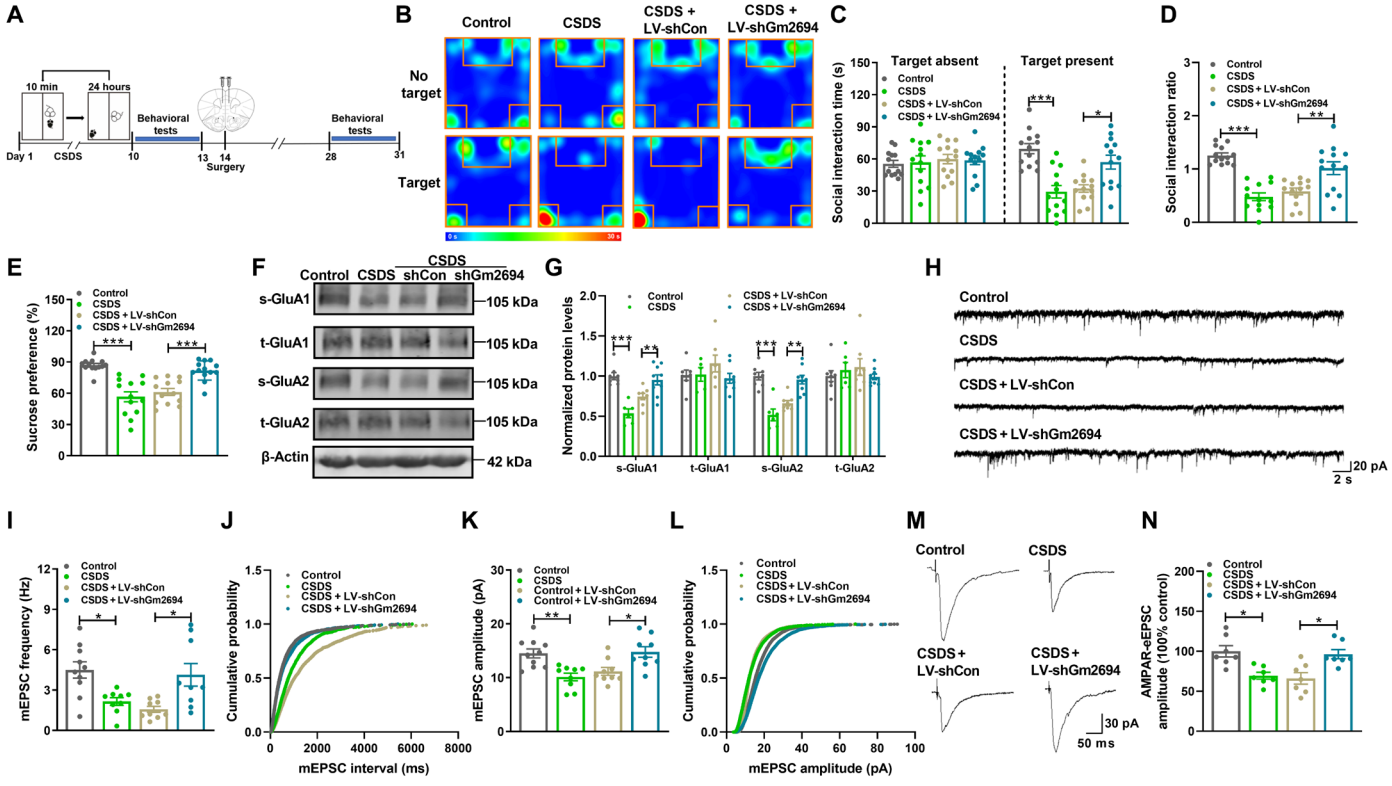

Fig. 2. Knockdown of Gm2694 in the mPFC prevents CSDS-induced depressive-like behaviors and enhances excitatory synaptic transmission. (**A**) The timeline of experimental procedure. (**B**) Heatmaps of time spent in the SIT. (**C**) LV-sh*Gm2694*–treated mice spent more time in the interaction zone when the target was present than LV-sh*Con*–treated mice ($n = 13$ mice per group). (**D**) LV-sh*Gm2694*–treated mice had a significant higher interaction ratio ($n = 13$ mice per group). (**E**) LV-sh*Gm2694*–treated mice displayed increased sucrose preference in SPT ($n = 13$ mice per group). (**F** and **G**) Western blotting results showing that LV-sh*Gm2694* treatment restored the surface expression of GluA1 and GluA2 in the mPFC of CSDS-treated mice ($n = 6$ to 9 mice per group). (**H**) Representative traces of AMPAR-mediated mEPSC recordings on the mPFC slices. Scale bar, 2 s, 20 pA. (**I** and **J**) Effect of LV-sh*Gm2694* on mEPSC frequency (I) and cumulative probability plots of mEPSC interevent intervals (J) recorded from representative cells in each group ($n = 9$ to 10 mice per group). (**K** and **L**) Effect of LV-sh*Gm2694* on mEPSC amplitude (K) and cumulative probability plots of mEPSC amplitude (L) from representative cells in each group ($n = 9$ to 10 mice per group). (**M**) Representative evoked AMPAR-mediated EPSCs (AMPAR-eEPSCs) traces in mPFC slices. Scale bar, 50 ms, 30 pA. (**N**) The amplitude of AMPAR-eEPSC was decreased in susceptible mice, and knockdown of Gm2694 significantly enhanced the amplitude of AMPAR-eEPSC in susceptible mice ($n = 7$ from five mice). All data are presented as the means ± SEM, with each point representing data from an individual. $^*P < 0.05$, $^{**}P < 0.01$, and $^{***}P < 0.001$ by one-way ANOVA (C, D, E, G, I, K, and N) followed by Bonferroni's post hoc test. The statistical details can be found in table S1.

rise time did not differ across groups (fig. S5, A and B). The density of dendritic spine in the mPFC was also decreased in the AAV-Gm2694 mice exposed to microdefeat stress compared with that of AAV-GFP mice (fig. S5, C and D). These results indicate that the elevated level of Gm2694 in the mPFC contributes to the increased susceptibility of mice to stress.

Gm2694 interacts with GRP78 in HT22 cells

Next, we performed an RNA pulldown assay followed by mass spectrometry analysis to identify Gm2694-associated protein in the mPFC that might be involved in synaptic transmission. It was found that the sense probe of Gm2694 was specifically associated with ER stress–related proteins, such as heat shock protein 90β (HSP90β), HSP90α, and GRP78 (fig. S6, A to D, and file S2). To determine whether these ER stress–related proteins, especially the UPR gatekeeper GRP78, play an important role in depressive-like behavior, we performed microarray analysis of gene expression in control and CSDS-treated mice and used gene set enrichment analysis for analysis of microarray data. The results showed that the UPR signal was up-regulated in the PFC of CSDS-treated mice (fig. S6, E and F). Furthermore, the expressions of HSP90α, HSP90β, and GRP78 proteins were analyzed by Western blotting, and the results showed that only GRP78 protein levels were increased in LV-sh*Gm2694*–treated mice exposed to CSDS compared with that of LV-sh*Con*–treated mice (fig. S6, G and H).

The assay of FISH showed a colocalization of Gm2694 and GRP78 in the cytoplasm of HT22 cells (Fig. 4A). RNA immunoprecipitation (RIP) assay in lysate of HT22 cells was performed to investigate whether GRP78 was associated with Gm2694. We found that compared with immunoglobulin G (IgG)–combined RNA, GRP78 was substantially enriched upon Gm2694 (Fig. 4, B and C). Similar results were observed in primary cultured cortical neurons (fig. S6I). RNA pulldown assay showed that biotin-Gm2694 was precipitated with GRP78 in the PFC of control mice (fig. S6J). Then, RIP was conducted to map in vivo Gm2694-GRP78 interactions. The results showed that CSDS increased the binding of Gm2694 to GRP78 in the mPFC of mice (Fig. 4D). An analysis of GRP78 intrinsic domains that required for Gm2694 binding was performed by catRAPID omics, which predicts RNA-protein associations and estimates the binding propensity of RNA-protein pairs (*39*). catRAPID analysis indicated that the 500– to 655–amino acid region of GRP78 was predicted

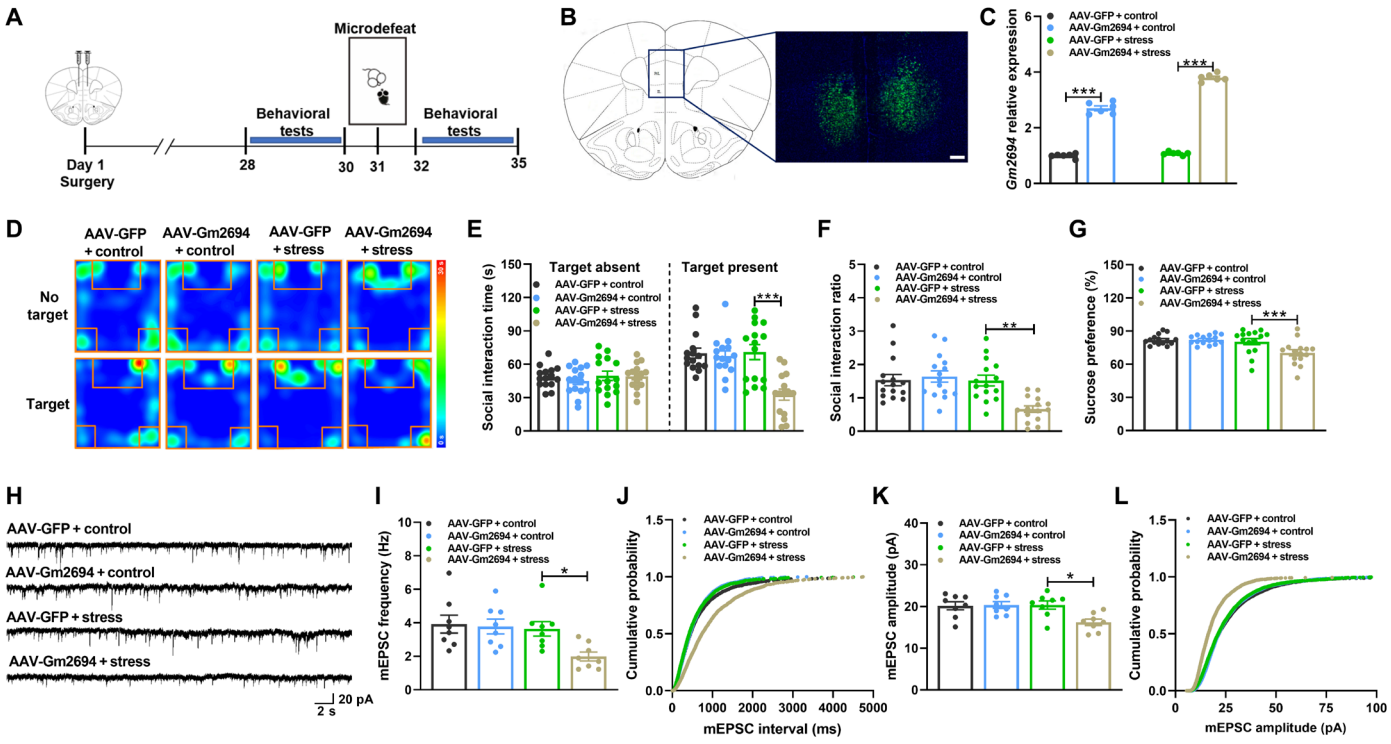

Fig. 3. Overexpression of Gm2694 in the mPFC facilitates the susceptibility of mice to stress and impairs excitatory synaptic transmission. (**A**) The timeline of experimental procedure. (**B**) Representative image of virus-mediated gene transfer in the mPFC of mice. Scale bar, 500 μm. (**C**) Four weeks after injection with AAV-GFP/AAV-Gm2694, quantitative reverse transcription polymerase chain reaction (qRT-PCR) was performed to assess the expression of Gm2694 in the mPFC of control and stressed mice ($n = 6$ mice per group). (**D**) Heatmaps of time spent in the SIT. (**E**) Overexpression of Gm2694 decreased interaction time of stressed mice ($n = 15$ mice per group). (**F**) Overexpression of Gm2694 decreased social interaction ratio of stressed mice ($n = 15$ mice per group). (**G**) Overexpression of Gm2694 decreased sucrose preference of stressed mice ($n = 15$ mice per group). (**H**) Representative traces of AMPAR-mediated mEPSC recordings on the mPFC neuron. Scale bar, 2 s, 20 pA. (**I** and **J**) Effect of AAV-Gm2694 on mEPSC frequency (I) and cumulative probability plots of mEPSC interevent intervals (J) from representative cells in each group ($n = 8$ mice per group). (**K** and **L**) Effect of AAV-Gm2694 on mEPSC amplitude (K) and cumulative probability plots of mEPSC amplitude (L) from representative cells in each group ($n = 8$ mice per group). All data are presented as the means ± SEM, with each point representing data from an individual. $^*P < 0.05$, $^{**}P < 0.01$, and $^{***}P < 0.001$ by two-way ANOVA (C, E, F, G, I, and K) followed by Bonferroni's post hoc test. The statistical details can be found in table S1.

to be the binding site to Gm2694 (Fig. 4, E and F). To further confirm this hypothesis, four additional constructs containing residues 1 to 655, 101 to 200, 1 to 100, 201 to 500, and 501 to 655 of GRP78 were made. It was found that the constructs containing residues 1 to 655 or 501 to 655 of GRP78 were bound to Gm2694, whereas the constructs containing residues 1 to 100 and 201 to 500 showed only weak binding to Gm2694, and the constructs containing residues 101 to 200 did not bind to Gm2694 (Fig. 4, G and H), indicating that Gm2694 mainly binds to the C-terminal domain (501 to 655 amino acids) of GRP78. To directly determine the interaction of Gm2694 with GRP78, fluorescence resonance energy transfer (FRET) microscopy was used in HT22 cells. By using Gm2694 FISH probe (red) and GRP78 antibody (green), it was found that Gm2694 was located in close proximity to GRP78 (6.713 ± 0.12 nm) with an FRET efficiency of 0.529 ± 0.02 (Fig. 4, I to K); on the contrary, incubation of HT22 cells with 18*S* probe illustrated that there was no obvious energy transfer, suggesting that Gm2694 directly interacts with GRP78.

CSDS induces the interaction between Gm2694 and GRP78 disrupting ER homeostasis

Given that there was the specific binding of Gm2694 to GRP78, we further examined the change in GRP78 protein level induced by CSDS. We found that the mRNA and protein expressions of GRP78 were increased in the mPFC of CSDS-treated mice (Fig. 5, A and B, and fig. S7A). Considering that activation of UPR-related protein, such as ATF6 and IRE1, could promote GRP78 gene transcription (*40*, *41*), the changes in stress-induced UPR expression were investigated. We found that the expressions of phosphorylated IRE1 (p-IRE1) and ATF6 proteins were increased in the mPFC of CSDS-treated mice, without alteration in the expression of apoptosis-related protein caspase-12 (Fig. 5C). Given that CSDS increased GRP78 expression in the mPFC and knockdown of Gm2694 also increased GRP78 expression in the mPFC of CSDS-treated mice, leading to antidepressant action, we wondered whether overexpression of Gm2694 in the mPFC could affect the expression of GRP78. Compared with that of normal mice treated with AAV-GFP, the levels of GRP78 and UPR-related protein were unchanged in the normal mice overexpressing Gm2694 (Fig. 5, D to F), suggesting that GRP78 may interact with three ER transducer sensors in the ER membrane. Next, both groups of mice were exposed to a microdefeat stress. It was found that overexpression of Gm2694 increased the expressions of GRP78, p-IRE1, and ATF6 in the mPFC of mice exposed to microdefeat stress, with no change in the expression of caspase-12 (Fig. 5, G to I), indicating that Gm2694 may bind to GRP78 in the ER lumen only under stress condition, where it disrupts the binding of GRP78 with UPR sensor proteins, resulting in prolonged activation of UPR and further increase in the expression of GRP78.

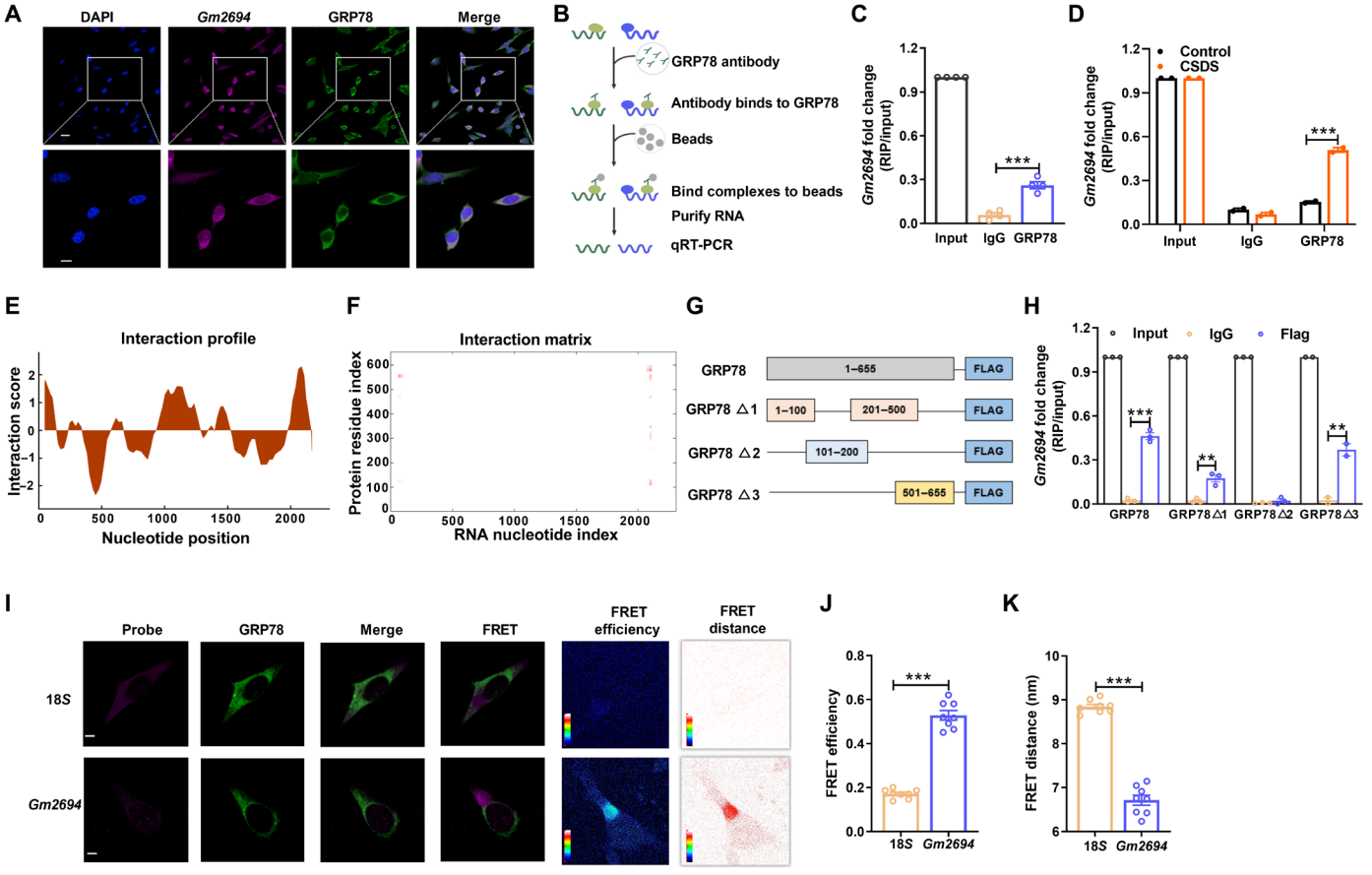

Fig. 4. Gm2694 interacts with GRP78 in HT22 cells. (**A**) Gm2694 colocalized with GRP78 in HT22 cells as shown by RNA FISH. Blue, 4′,6-diamidino-2-phenylindole (DAPI); red, Gm2694; green, GRP78. Scale bars, 20 μm (top) and 5 μm (bottom). (**B**) Experimental procedure of RIP. (**C**) RIP and subsequent qRT-PCR assay showing that GRP78 interacted with Gm2694 in HT22 cells ($n = 4$). (**D**) RIP and subsequent qRT-PCR assay showing that CSDS increased the binding of Gm2694 to GRP78 in the mPFC ($n = 2$). (**E**) The interaction profile that represented the protein interaction score (*y* axis) relative to the Gm2694 RNA sequence (*x* axis) provided information about the region most likely to be bound by the protein. (**F**) The interaction matrix showing a heatmap of the GRP78 protein (*y* axis) and Gm2694 RNA (*x* axis) regions. (**G**) Schematics of GRP78 wild-type and truncated constructs. (**H**) RIP assays in HT22 cells transfected with Flag-Vector or Flag-GRP78 wild-type and truncated constructs ($n = 2$ to 3). (**I** to **K**) Confocal FRET microscopy and analysis showing that Gm2694 was located in close proximity to GRP78 ($n = 8$). Scale bars, 5 μm. All data are presented as the means ± SEM, with each point representing data from an individual. $^{**}P < 0.01$ and $^{***}P < 0.001$ by one-way ANOVA (C and H) or two-way ANOVA (D) followed by Bonferroni's post hoc test or Student's *t* test (J and K). The statistical details can be found in table S1.

To further verify this hypothesis, we applied the ER stress activator tunicamycin (TM) at the indicated dosage in HT22 cells. After exposure to TM for 2, 4, or 8 hours, TM (1, 2, and 4 μg/ml) dose-dependently increased the expression of GRP78; however, the expression of caspase-12 was only elevated in HT22 cells treated with TM (4 μg/ml) for 8 hours (fig. S7, B and C). Thus, TM was given by the dosage of 2 μg/ml for 4 hours in the further study. It was shown that administration of TM into the primary cultured cortical neurons increased the expression of GRP78, p-IRE1, and ATF6, but not caspase-12 (fig. S8, A to C). However, overexpression of Gm2694 (LV-Gm2694) in primary cortical neurons did not change the expression of GRP78 and UPR signaling (fig. S8, D to F), which may be due to the binding of GRP78 with UPR protein in the ER membrane. While Gm2694 was overexpressed in primary cortical neurons before TM treatment, TM increased the expression of GRP78 regardless of the presence or absence of Gm2694 (fig. S8, G and H). Overexpression of Gm2694 followed by TM treatment did not further elevate the expression of GRP78 protein, indicating that Gm2694 binds to GRP78, liberating from UPR protein into the ER lumen under TM treatment. Together, these results indicate that CSDS promotes the binding of Gm2694 to GRP78, resulting in increased expression of GRP78 by activation of UPR signaling.

Stress-induced activation of Gm2694-GRP78 complex decreases the surface expression of AMPAR

Previous studies have reported that GRP78 recognizes and binds to GluA1 and GluA2 subunits of AMPAR (*28*–*30*) and regulates AMPAR postsynaptic trafficking and localization (*28*, *42*). In the present study, Western blotting analysis showed that CSDS reduced the surface expressions of GluA1 and GluA2 in the mPFC but did not affect the total expressions of GluA1 and GluA2 subunits of AMPAR (Fig. 6, A and B). We then asked whether Gm2694 overexpression could decrease the surface expression of AMPAR in the mPFC of mice exposed to a microdefeat stress. It was found that the surface expressions of GluA1 and GluA2 were reduced in the mPFC of AAV-Gm2694–treated mice exposed to microdefeat stress (Fig. 6, C and D).

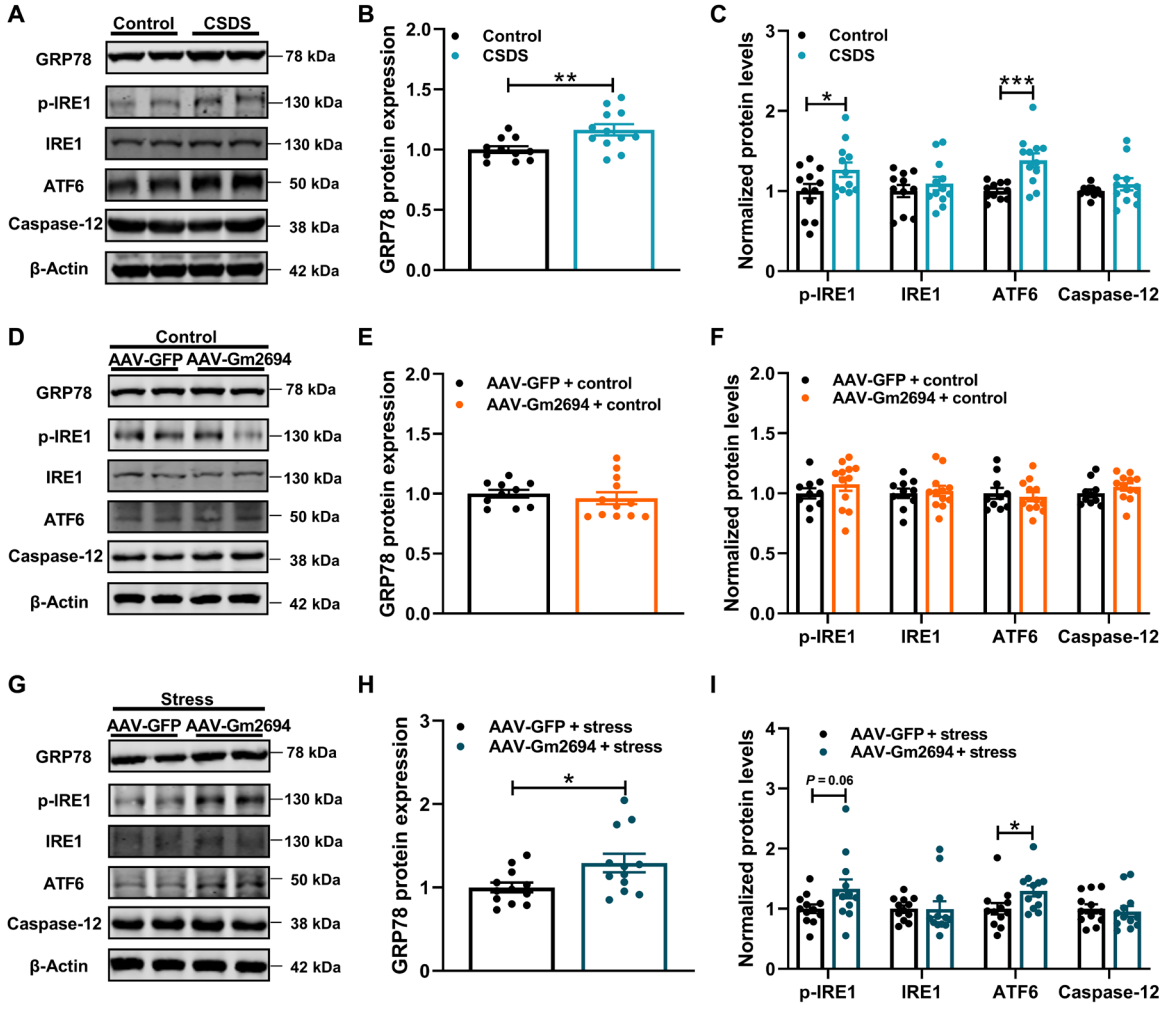

Fig. 5. Gm2694 interacts with GRP78 under stress condition. (**A**) Representative images of Western blotting in control and CSDS-treated mice. (**B**) The expression of GRP78 protein was increased in the mPFC of CSDS-treated mice ($n = 11$ to 12 mice per group). (**C**) The expressions of p-IRE1 and ATF6 proteins were increased in the mPFC of CSDS-treated mice ($n = 11$ to 12 mice per group). (**D**) Representative images of Western blotting in AAV-Gm2694–treated unstressed mice. (**E**) Overexpression of Gm2694 in the mPFC did not change the expression of GRP78 protein in unstressed mice ($n = 10$ to 12 mice per group). (**F**) UPR was unaltered by overexpression of Gm2694 in the mPFC of unstressed mice ($n = 10$ to 12 mice per group). (**G**) Representative images of Western blotting in AAV-Gm2694–treated stressed mice. (**H**) Overexpression of Gm2694 in the mPFC increased the expression of GRP78 in stressed mice ($n = 12$ mice per group). (**I**) Overexpression of Gm2694 in the mPFC resulted in the increased expressions of p-IRE1 and ATF6 in stressed mice. $n = 12$ mice per group. All data are presented as the means ± SEM, with each point representing data from an individual. $^*P < 0.05$, $^{**}P < 0.01$, and $^{***}P < 0.001$ by Student's t test (B, C, E, F, H, and I). The statistical details can be found in table S1.

Considering that administration of TM into primary cortical neurons induces the expression of GRP78, we then examined the impact of up-regulation of GRP78 on the surface expression of AMPAR. As shown in Fig. 6 (E and F), the surface expression of GluA1 and GluA2 was significantly higher in TM-treated neurons than that of control neurons. However, pretreatment with Gm2694 overexpression blocked the TM-induced increase in the surface expression of GluA1 and GluA2 subunits of AMPAR (Fig. 6, G to I). In addition, an in vivo experiment was conducted to test the effect GRP78 on AMPAR under chronic stress. It was shown that overexpression of GRP78 (AAV-GRP78) in the mPFC reversed the decrease in surface expression of GluA2 induced by CSDS, with no obvious changes in the total levels of GluA1 or GluA2 (Fig. 6, J and K). Together, these results indicate that chronic stress may cause the interaction of Gm2694 with GRP78, resulting in decreased surface expression of the GluA1 and GluA2 subunits of AMPAR.

GRP78 regulates chronic stress–induced depressive-like behaviors of mice by modulating excitatory synaptic transmission

To determine the role of GRP78 in chronic stress–induced depressive-like behaviors, we injected LV-*shGRP78* into the mPFC to inhibit GRP78 expression (fig. S9, A and B). Two weeks later, mice were exposed to a microdefeat stress (Fig. 7A), and LV-*shGRP78*–treated mice displayed a significant reduction in social interaction and sucrose preference after microdefeat stress compared with those of LV-*shCon* mice (Fig. 7, B to D, and fig. S9C). The amplitude of mEPSC was decreased in the LV-*shGRP78*–treated mice exposed to

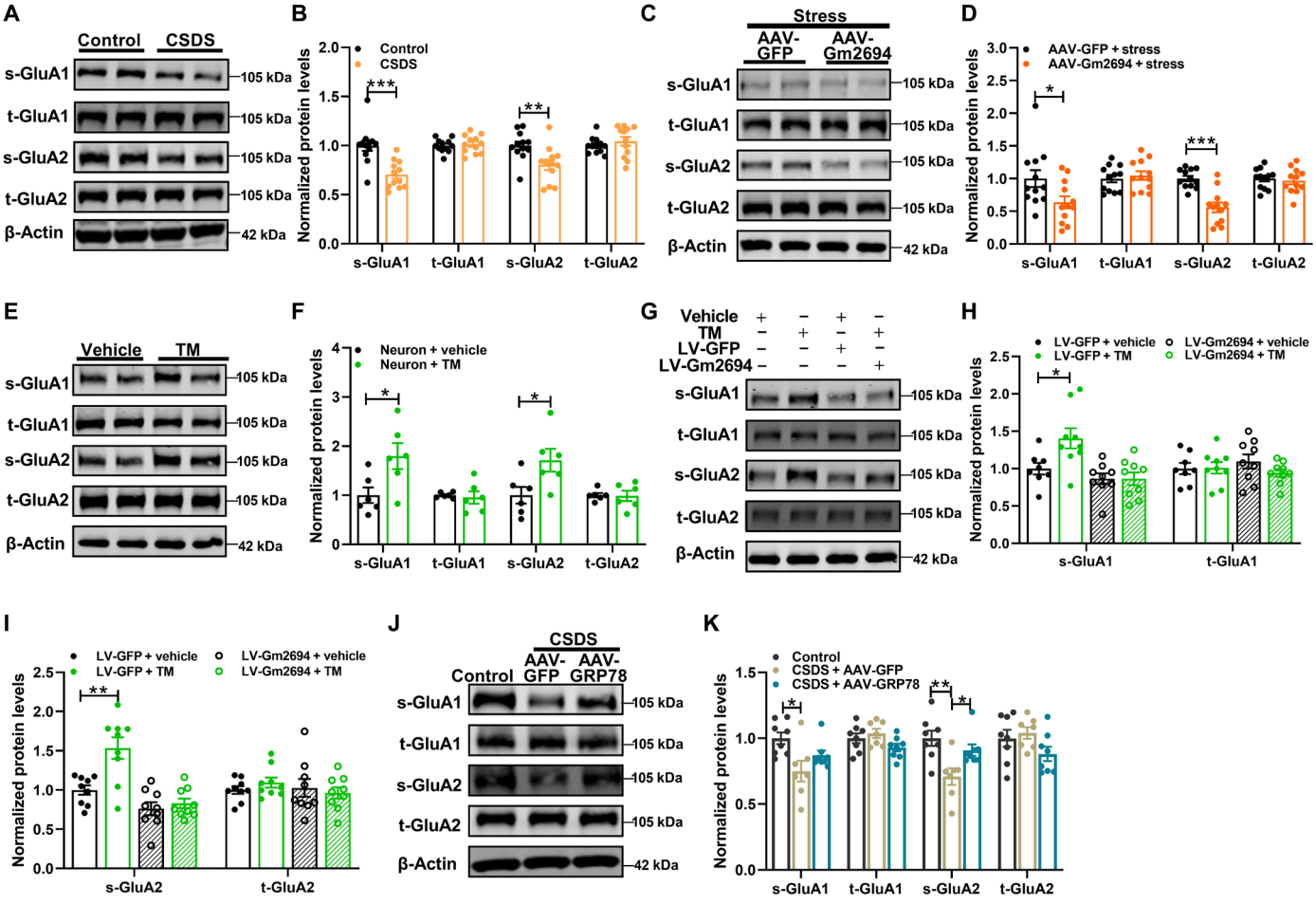

Fig. 6. CSDS-induced interaction of Gm2694 and GRP78 decreases surface expression of AMPAR. (**A**) Representative images of Western blotting in CSDS-treated mice. (**B**) CSDS decreased surface expression of GluA1 and GluA2 in the mPFC ($n = 12$ mice per group). (**C**) Representative images of Western blotting in AAV-Gm2694–treated stressed mice. (**D**) Overexpression of Gm2694 in the mPFC decreased surface expression of GluA1 and GluA2 in stressed mice ($n = 12$ mice per group). (**E**) Representative images of Western blotting in TM-treated primary cultured cortical neurons. (**F**) TM increased surface expression of GluA1 and GluA2 in primary cortical neurons ($n = 6$ cells per group). (**G**) Representative images of Western blotting in primary cultured cortical neurons treated with TM and LV-Gm2694. (**H**) Overexpression of Gm2694 in primary cortical neurons blocked TM-induced increase in surface expression of GluA1 ($n = 8$ to 9 cells per group). (**I**) Overexpression of Gm2694 in primary cortical neurons blocked TM-induced increase in surface expression of GluA2 ($n = 9$ cells per group). (**J**) Representative images of Western blotting in AAV-GRP78–treated stressed mice. (**K**) Western blotting results showing the effects of AAV-GRP78 on CSDS-induced surface expression of GluA1 and GluA2 in the mPFC ($n = 7$ to 8 mice per group). All data are presented as the means ± SEM, with each point representing data from an individual. $^*P < 0.05$, $^{**}P < 0.01$, and $^{***}P < 0.001$ by one-way ANOVA (K) or two-way ANOVA (H and I) followed by Bonferroni's post hoc test or Student's *t* test (B, D, and F). The statistical details can be found in table S1.

microdefeat stress compared with that in LV-sh*Con* mice (Fig. 7, E to I), without changes in the decay time and rise time (fig. S9, D and E). The density of dendritic spine in the mPFC was also reduced in the LV-*shGRP78*–treated mice that received microdefeat stress compared with that in LV-sh*Con* mice (fig. S9, F and G). These results suggest that the decrease in GRP78 protein in the mPFC facilitates the susceptibility of mice to stress.

On the contrary, overexpression of GRP78 increased the social interaction of defeated mice in SIT (Fig. 7, J to L, and fig. S10, A to C) and restored the sucrose preference of defeated mice (Fig. 7M), but not in control mice (fig. S10, D to F), suggesting that overexpression of GRP78 in the mPFC attenuates CSDS-induced depression-like behaviors. In addition, overexpression of GRP78 in the mPFC reversed the reduction of both amplitude and frequency of AMPAR-mediated mEPSCs induced by CSDS (Fig. 7, N to R). However, overexpression of GRP78 in the mPFC did not affect excitatory synaptic transmission in control mice (fig. S11, A to E). There were no obvious changes in the decay time and rise time at excitatory synapses onto mPFC neurons in all groups (fig. S12, A and B). Furthermore, CSDS-induced reduction in the density of dendritic spine was prevented by injection of AAV-GRP78 into the mPFC (fig. S12, C and D), indicating that overexpression of GRP78 alleviates CSDS-induced synaptic deficit in the mPFC.

DISCUSSION

In the present study, we have identified the role of a previously unidentified lncRNA Gm2694 in depressive-like behaviors of male mice. CSDS induced an increase in lncRNA Gm2694 in the mPFC, and knockdown of Gm2694 prevented CSDS-induced depressive-like behaviors via enhancing excitatory synaptic transmission. The evidence supports that Gm2694 directly interacted with C-terminal

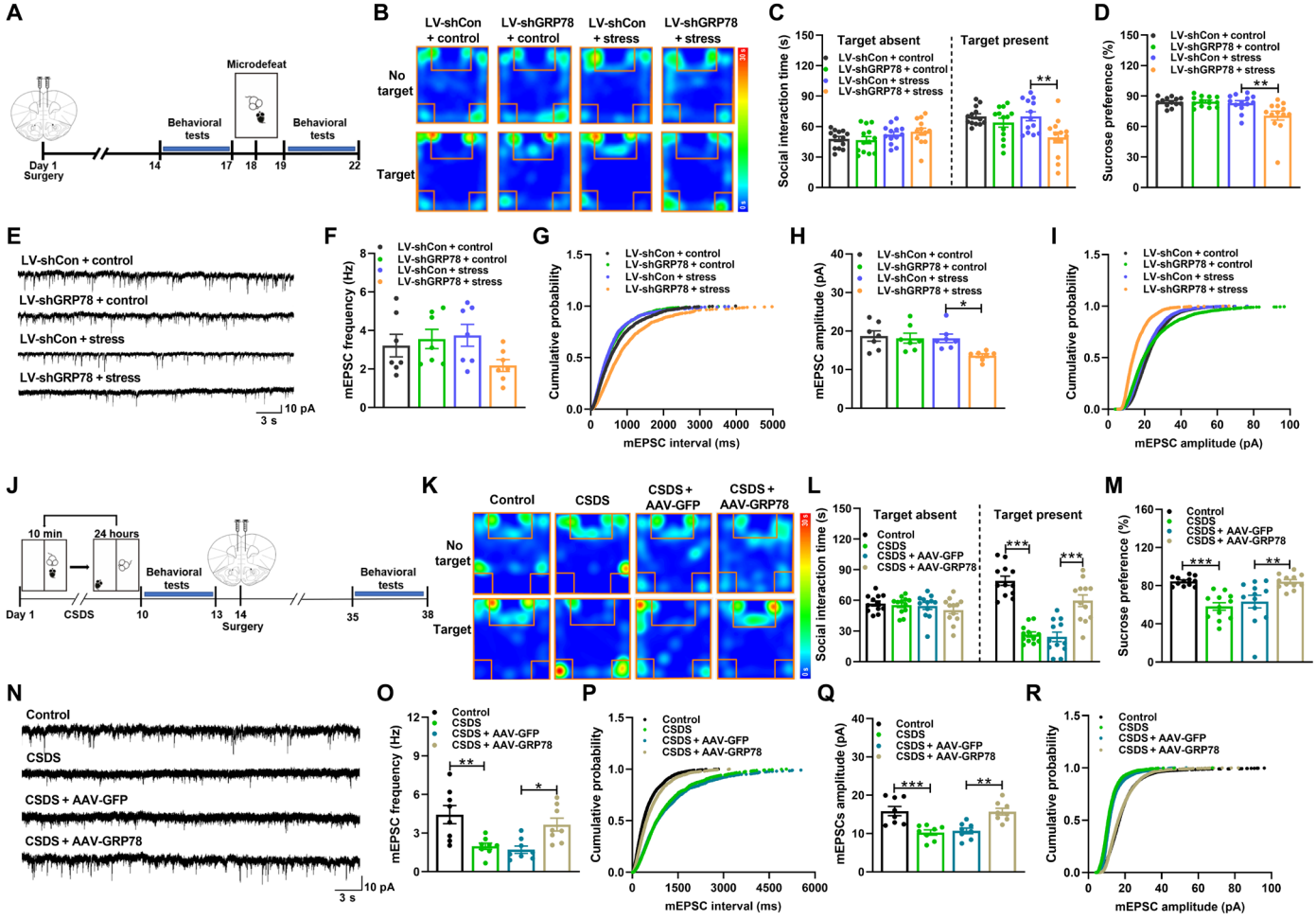

Fig. 7. GRP78 regulates depressive-like behaviors of mice by modulating excitatory synaptic transmission. (**A**) The timeline of experimental procedure. (**B**) Heatmaps of time spent in the SIT. (**C**) Knockdown of GRP78 decreased interaction time of stressed mice ($n = 12$ to 13 mice per group). (**D**) Knockdown of GRP78 decreased sucrose preference of stressed mice ($n = 12$ to 13 mice per group). (**E**) Representative traces of AMPAR-mediated mEPSC recordings on mPFC neurons. Scale bar, 3 s, 10 pA. (**F** and **G**) Effect of LV-shGRP78 on mEPSC frequency (F) and cumulative probability plots of mEPSC interevent intervals (G) from representative cells in each group ($n = 7$ mice per group). (**H** and **I**) Effect of LV-shGRP78 on mEPSC amplitude (H) and cumulative probability (I) from representative cells in each group ($n = 7$ mice per group). (**J**) The timeline of experimental procedure. (**K**) Heatmaps of time spent in the SIT. (**L**) AAV-GRP78–treated stressed mice spent more time in the interaction zone ($n = 12$ mice per group). (**M**) AAV-GRP78–treated stressed mice exhibited increased sucrose preference ($n = 12$ mice per group). (**N**) Representative traces of AMPAR-mediated mEPSC recordings on the mPFC neuron. Scale bar, 3 s, 10 pA. (**O** and **P**) Effect of AAV-GRP78 on mEPSC frequency (O) and cumulative probability plots of mEPSC interevent intervals (P) from representative cells in each group ($n = 8$ mice per group). (**Q** and **R**) Effect of AAV-GRP78 on mEPSC amplitude (Q) and cumulative probability plots of mEPSC amplitude (R) from representative cells in each group ($n = 8$ mice per group). All data are presented as the means ± SEM, with each point representing data from an individual. $^*P < 0.05$, $^{**}P < 0.01$, and $^{***}P < 0.001$ by two-way ANOVA (C, D, F, and H) or one-way ANOVA (L, M, O, and Q) followed by Bonferroni's post hoc test. The statistical details can be found in table S1.

domain of GRP78, a major ER molecular chaperone involved in ER homeostasis, in the ER lumen under stress condition, leading to the abrogation of GRP78 function, disruption of ER homeostasis, and decrease in surface expression of AMPARs. Furthermore, we found that overexpression of GRP78 in the mPFC promoted surface expression of AMPARs and attenuated CSDS-induced depressive-like behaviors. This study highlights the role of lncRNAs in depressive-like behaviors and provides new insight into the potential target for the treatment of depression.

Numerous noncoding RNAs, especially microRNAs and circular RNAs, have been found to be involved in neuronal function and psychiatric disorders, such as depression (*35*, *43*–*45*), but little is known about lncRNA function in these processes. Recent study has demonstrated that 30% of differentially expressed genes in patients with depression are lncRNAs (*19*). For example, LINC00473, an lncRNA with a sex-specific role in depression that localized in the nucleus of neurons, is down-regulated in cortex of depressed females (*19*). Through lncRNA microarray assay, we found that the level of Gm2694 was enriched in the cytoplasm and increased in the mPFC induced by CSDS. There was a positive correlation between Gm2694 level and depressive-like behaviors, and knockdown of Gm2694 expression in the mPFC ameliorated depressive-like behaviors. On the contrary, the elevation of Gm2694 expression in the mPFC promoted stress susceptibility of mice, suggesting that Gm2694 in the mPFC is a critical regulator of stress susceptibility. However, the exact mechanism underlying chronic stress–induced increase in Gm2694 expression

was largely unknown. It has been demonstrated that epigenetic regulation of chromatin remodeling likely plays a prominent role in chronic stress–induced behavioral changes (*46*). Super-enhancers are large clusters of DNA elements, which can physically contact with their target promoters by chromatin looping during transcription, and recruit a complex array of transcriptional coactivators to affect transcriptional activation. It has been reported that super-enhancers play a primary role in chronic stress–associated intestinal barrier dysfunction (*47*). Therefore, we proposed that chronic stress may facilitate the binding of super-enhancers to transcriptional coactivators and drive the transcriptional activation of Gm2694, leading to the upregulation of Gm2694. In addition, increasing evidence shows that chronic stress alters the expression of epigenetic enzymes and associated histone posttranslational modifications and DNA methylation in several brain regions. Thus, chronic stress may upregulate the level of Gm2694 via increasing the histone acetylation or inhibiting the methylation in the promoter region of Gm2694, which needed further investigation.

To investigate whether lncRNA Gm2694 had a human analog, we performed the analysis of sequence homology between human and mouse lncRNA. The genomic position of the homologous sequences of Gm2694 in the human reference genome was predicted to be localized in chr16: 49280333 to 49327853 (hg38), where the gene encoding cerebellin 1 (CBLN1) and noncoding RNA RP11-491F9.1 were located on. The result of similarity in sequence alignment showed that Gm2694 [2302 base pairs (bp)] and RP11-491F9.1 (654 bp) had 21.98% sequence similarity and the nucleotide sequence of 350- to 1320-bp region of Gm2694 and noncoding RNA RP11-491F9.1 shared about 48% similarity, indicating that Gm2694 is, at least in part, evolutionarily conserved between mice and human.

Although several lncRNAs have been functionally annotated in the central nervous system, the majority remains to be characterized. The specific regulatory mechanism of lncRNA can be predicted by its cellular localization (*48*). The lncRNAs located in the cell nucleus can participate in the regulation of transcription, epigenetic modification, and genome stability in neurons (*10*–*12*, *19*, *49*, *50*). However, little is known about the function of cytoplasmic lncRNAs. A recent study of subcellular fractionation assay has shown that lncRNA Gm2694 is located in the cytoplasm of embryonic stem cells (*51*); however, the isoform 204 of lncRNA Gm2694 [lncRNA-Promoting Methylation (lncRNA-PM)] that is located in the nucleus regulates Cbln1 transcriptional activation through an isoform-specific manner (*52*), suggesting that lncRNA Gm2694 functions in a different way from other Gm2694 isoform (lncRNA-PM) and sheds light on the biological significance of lncRNA-based isoform in nervous system. In our study, the result of FISH assay showed that Gm2694 was abundant in the cytoplasm, demonstrating that Gm2694 exerts its function in the cytoplasm. RNA-centric techniques are often required to explore the unknown functions of lncRNAs. RNA pulldown is the most widely used method to identify lncRNA-interacting proteins (*53*). We found that Gm2694 interacted with GRP78, which is the major ER residential chaperone and consists of an N-terminal adenosine 5′-triphosphate (ATP)–binding domain and a C-terminal substrate-binding domain (*54*). Under physiological condition, GRP78 binds to the ER-luminal domain of ATF6 and IRE1 via its substrate-binding domain and then blocks UPR activation (*26*). lncRNAs can act as molecular decoys to bind and titrate away targeted proteins (*55*); therefore, lncRNAs that fit into this functional model could presumably act by negative regulation of an effector. Our results showed that Gm2694 preferentially interacted with C-terminal domain of GRP78 including binding domain, which led to the abrogation of GRP78 function. Furthermore, both knockdown of Gm2694 and overexpression of GRP78 attenuated depressive-like behaviors, indicating that Gm2694 can act as molecular decoy that competitively binds to GRP78 protein.

GRP78 plays an important role in maintaining ER homeostasis and synaptic plasticity (*27*, *56*). In the early stage of ER stress, GPR78 is competitively titrated by the accumulation of unfolded proteins, and the substrate-binding affinity is increased for correctly folded proteins. Activation of ER stress triggers UPR signaling cascade and leads to increased expression of GRP78 (*26*). Overexpression of GRP78 attenuates ER stress by enhancing protein folding and maintaining IRE1 and ATF6 in their inactive states, which contributes to the maintenance of ER homeostasis (*54*). Both clinical and preclinical studies have shown that the expression of UPR genes and GRP78 mRNA is up-regulated in multiple brain regions of depression, including PFC (*32*, *57*), temporal cortex (*31*), and dentate gyrus (*58*), implicating that GRP78 is an important factor in the pathogenesis of depression. Our results are consistent with previous findings that the expression of GRP78 was increased in the mPFC of CSDS-treated mice, and GRP78 overexpression in the mPFC ameliorated the depressive-like behaviors. To further analyze these seemingly contradictory results, we microinjected the mice with AAV-Gm2694 into the mPFC and subsequently exposed to a microdefeat stress. It was found that administration of AAV-Gm2694 increased the expression of GRP78 and UPR signaling and promoted the depressive-like behaviors, illustrating that GPR78 may competitively titrate by accumulated Gm2694 in the ER lumen under stress condition. Moreover, ER stress–activated UPR signaling further increased the expression of GRP78, which may be decoyed by Gm2694 in the ER lumen. Together, chronic stress induced the elevation of Gm2694, which interacted with GRP78 and kept GRP78 sequestered in the ER lumen, resulting in the impairment of proper folding of proteins and the disruption of ER homeostasis.

Recently, the dysfunction of AMPARs has been recognized to be involved in depression, and AMPARs are down-regulated across multiple brain regions in depression, such as hippocampus (*20*) and mPFC (*22*). Our findings demonstrated that the surface expressions of GluA1 and GluA2 were decreased in the mPFC of CSDS-treated mice. UPR signaling is needed for AMPARs assembly and trafficking (*24*, *59*), for example, mutation of IRE1 blocks the trafficking of GluA1 and GluA2 and promotes the assembly of AMPARs in the ER (*59*). Loss of IRE1 causes abnormal morphogenesis of dendrites, which is reversed by overexpression of GRP78 (*56*). Vandenberghe *et al.* (*24*) reported that transfection of COS7 cells with constitutively active ATF6 enhanced the level of GRP78 and surface expression of GluA1 subunit. Colocalization of GRP78 with GluA1 and GluA2 subunits has been observed by electron microscopy (*29*) and immunofluorescence (*28*), suggesting that GRP78 may mediate the release of AMPAR from ER to plasma membrane. In our results, TM-mediated UPR signaling increased the expression of GRP78 and promoted surface expression of GluA1 and GluA2 subunits in primary cultured cortical neurons. Similarly, overexpression of GRP78 in the mPFC increased the surface expression of AMPARs and AMPAR-mediated mEPSCs and the density of dendritic spine, leading to the attenuation of depressive-like behaviors. Kuijpers *et al.* (*60*) reported that selective accumulation of tubular ER in axons results in increased excitatory neurotransmission. We also observed that overexpression

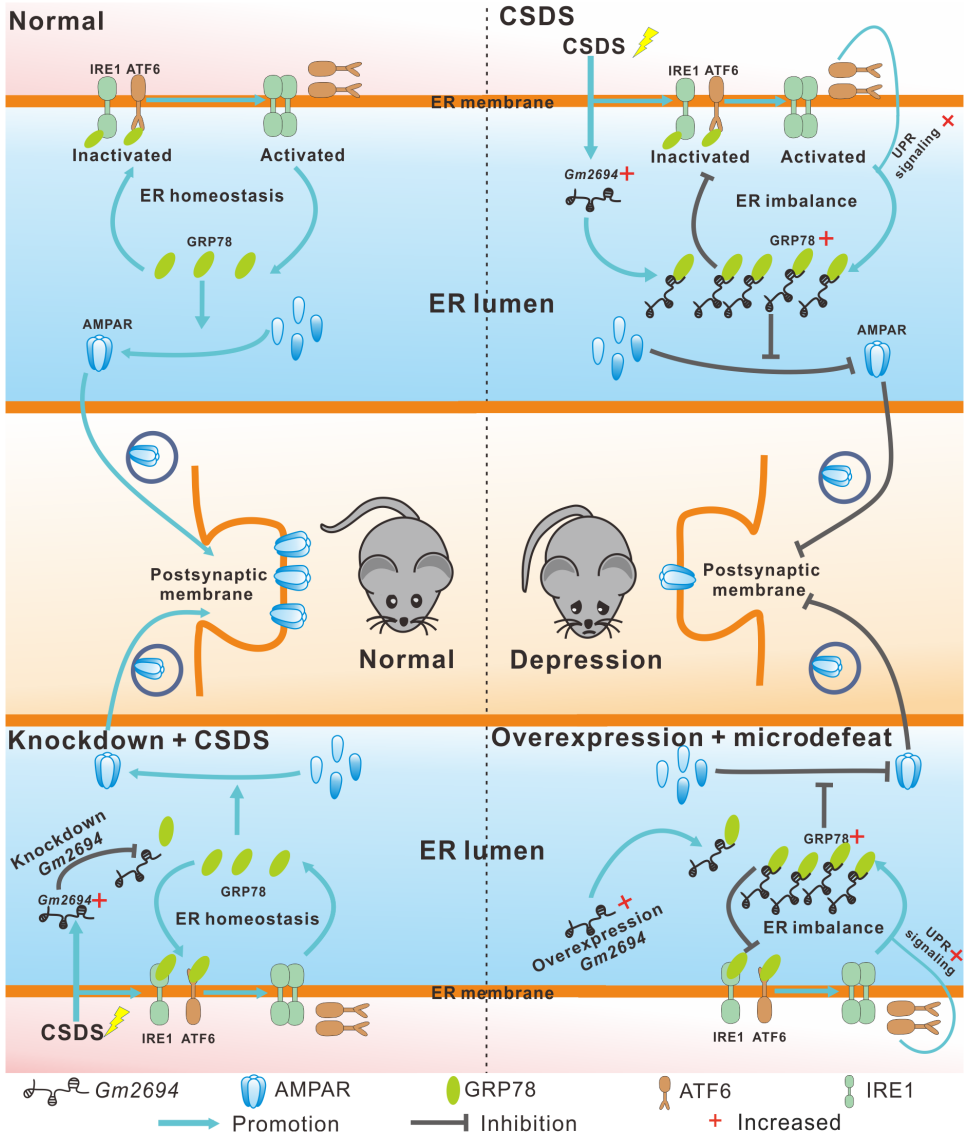

Fig. 8. Working model of Gm2694 in depression. In normal mice, a stressful event leads to an ER stress response. In the early stage of ER stress, GPR78 releases from ER membrane to ER lumen, activates UPR signaling, indicated by dimerization of IRE1 and translocation of ATF6, and increases the surface expression of AMPARs. In the late stage of ER stress, GRP78 returns to the ER membrane, binds to IRE1 and ATF6, and keeps them in their inactive states, contributing to the maintenance of ER homeostasis. CSDS increased Gm2694 expression, and Gm2694 interacts with GRP78 to restrict the function of GRP78. As a result, GRP78 is sequestered in ER lumen and fails to bind to IRE1 and ATF6, resulting in ER imbalance. On the other hand, the Gm2694-GRP78 complex impedes the trafficking of postsynaptic AMPAR. Overexpression of Gm2694 causes Gm2694 to interact with GRP78 under the microdefeat conditions. As a result, GRP78 becomes trapped in the ER lumen and is unable to bind to IRE1 and ATF6, resulting in an ER imbalance. Simultaneously, the Gm2694-GRP78 complex inhibits postsynaptic AMPAR trafficking. Knockdown of Gm2694 following CSDS can result in GRP78 release from the Gm2694-GRP78 complex. The unbound GRP78 in the ER lumen promotes postsynaptic AMPAR trafficking. Meanwhile, GRP78 returns to the ER membrane to block UPR signaling.

of GRP78 in the mPFC increased the frequency and amplitude of AMPAR-mediated mEPSC of CSDS-treated mice. Together, our results indicate that the increase in GRP78 expression in the mPFC enhances AMPAR-mediated synaptic transmission and ameliorates depressive-like behaviors.

There are only a few studies that explore the relationship between lncRNAs and ER homeostasis (*33*, *34*, *61*); however, lncRNA-regulated ER homeostasis has not been implicated in central nervous system. Our study provides the first evidence for the role of lncRNA Gm2694 in depressive-like behaviors by regulation of ER homeostasis via interaction with GRP78. So far, knowledge of the effects of lncRNAs on synaptic transmission is still unexpectedly limited. Previous studies show that NeuroLNC (*62*), a neuron-specific nuclear lncRNA, orchestrates neuronal excitability by influencing presynaptic function. lncRNA AtLAS (*63*) regulates social hierarchy by controlling postsynaptic AMPAR trafficking. In this study, we showed that lncRNA Gm2694 impaired AMPAR-mediated synaptic transmission via disrupting ER homeostasis. Knockdown of Gm2694 in the mPFC promoted the surface expression of GluA1 and GluA2, enhanced the frequency and amplitude of AMPAR-mediated mEPSCs, and

ameliorated depressive-like behaviors. On the contrary, overexpression of Gm2694 blocked GRP78-mediated surface expression of AMPARs and impaired AMPAR-mediated mEPSCs. These results indicate that Gm2694 plays a key role in both ER homeostasis and synaptic transmission.

Together, our findings revealed that Gm2694 bound with C-terminal domain of GRP78 and acted as molecular decoy to inhibit GRP78 function, which disrupted ER homeostasis, resulting in decreased surface expression of AMPARs and density of dendritic spine, thus facilitating the susceptibility of mice to chronic stress (Fig. 8). Our study identified lncRNA Gm2694 as a promising therapeutic target for MDD and unraveled the mechanism of lncRNA Gm2694 underlying the regulation of chronic stress–induced synaptic deficits.

MATERIALS AND METHODS

Animals

Adult male C57BL/6J mice (7 to 8 weeks old) were purchased from Hunan SJA Laboratory Animal Corporation Ltd. (Changsha, Human province, China), and CD-1 mice (7 to 10 months old) were purchased from Vital River Laboratories (Beijing, China). All mice were given 7 days to acclimate before experimentation and randomly assigned to experimental groups. All animals were maintained on a 12-hour light/12-hour dark cycle at a constant temperature (23° ± 2°C) and humidity (50 ± 10%). Food and water were available ad libitum. All animal procedures were performed in strict accordance with the Animal Research: Reporting of In Vivo Experiments Guidelines. All experimental procedures were approved by the Animal Welfare Committee of Huazhong University of Science and Technology.

Social defeat stress procedures

Chronic social defeat stress

CSDS was carried out as previously reported (*20*). Briefly, CD-1 mice were screened for aggressive behavior by 3-day screening process. Every day, C57BL/6J mice were exposed to a different CD-1–resident aggressor mouse for 10 min. C57BL/6J mice were separated from the aggressor and placed across a plastic separator with holes. Control C57BL/6J mice were housed individually. After 10 days of CSDS, mice underwent behavior tests.

Microdefeat stress

The microdefeat protocol is a subthreshold variation of the CSDS protocol, which was used to evaluate increased susceptibility to stress (*38*). The C57BL/6J mouse is subjected to subthreshold levels of social defeat that consist of three 5-min defeat sessions, each separated by a 15-min period of rest. The behavior tests were conducted 24 hours later.

Behavioral tests

Social interaction test

SIT is used to assess social avoidance behavior as previously described with minor modifications (*64*). All tests were performed under red light condition. During the first 2.5-min stage (target absent), experimental C57BL/6J mouse was allowed to explore freely an open-field arena (42 cm by 42 cm by 42 cm), containing a wire-mesh cage (10 cm by 6 cm) opposed to one side. Their movements were monitored and recorded using ANY-maze software (Stoelting, Co, USA). At the end of 2.5 min, the C57BL/6J mouse was removed, and the arena was cleaned. During the second 2.5-min stage (target present), the C57BL/6J mouse was reintroduced into this arena, with an unfamiliar CD-1 aggressor mouse within the cage. SIT behavior was calculated as total time spent by the C57BL/6J mouse in the interaction zone when the target was absent or present or as a ratio (time spent in the interaction zone in the presence versus absence of the target).

Sucrose preference test

SPT was performed as previously described with some modifications (*64*). Mice were habituated to two identical 50-ml tubes containing 1% sucrose solution and water for 48 hours. After the first 24 hours, the positions of tubes were switched to eliminate potential side bias. Then, mice were deprived of water for 12 hours. The tubes were again weighed, and the sucrose preference ratio was calculated for the final 12 hours of testing. The sucrose preference was calculated by dividing the total amount of sucrose solution by the total amount of fluid (water + sucrose) consumed.

Quantitative reverse transcription polymerase chain reaction

For quantitative reverse transcription polymerase chain reaction (qRT-PCR), total RNA was extracted from different tissues and cell lines using TRIzol reagent (Invitrogen, Carlsbad, CA), according to the manufacturer's instructions, and treated with excess deoxyribonuclease I (TransGen Biotech, Beijing, China). Cytoplasmic RNA separation was performed using a cytoplasmic and nuclear RNA purification kit (Norgen Biotek, ON, Canada). First-strand cDNA synthesis was generated using the RevertAid First-Strand cDNA Synthesis Kit (Fermentas, Thermo Fisher Scientific, Canada). qRT-PCR was performed to measure RNA expression levels with the SYBR Premix Ex Taq Kit (Takara, Dalian, China). Reactions were performed in 96-well plates in the StepOnePlus Real-Time PCR System (Applied Biosystems, Foster City, CA). PCR amplification consisted of denaturation at 95°C for 30 s, followed by 40 cycles at 95°C for 50 s and 60°C for 30 s. The primer sequences were used as follows: *Gm2694*, 5′-CAACATCTCCTTATCCGC-3′ (forward) and 5′-CACCTCTAACCTCTGGCT-3′ (reverse); *Grp78*, 5′-GATGTTTGTCCCCTTACACT-3′ (forward) and 5′-CAACCTTCATAGACCTTGATT-3′ (reverse); *Gapdh*, 5′-ATGGTGAAGGTCGGTGTG-3′ (forward) and 5′-CATTCTCGGCCTTGACTG-3′ (reverse).

lncRNA microarray analysis

Total RNAs were isolated with TRIzol reagent from mPFC. The microarray profiles were carried out by the Agilent Mouse lncRNA array 8 × 60,000 (Oebiotech, Shanghai, China). RNA samples (200 ng) were reverse-transcribed into cDNA, and cDNA samples were labeled with cyanine-3–cytidine 5′-triphosphate and used as probes for hybridization on the lncRNA microarray, which was then scanned with an Agilent microarray scanner. Agilent Feature Extraction software (version 11.0.1.1) was used to analyze the acquired array images. GeneSpring software (version 12.0, Agilent Technologies, Santa Clara, CA) was used to finish the basic analysis with the raw data. The threshold set for the up-regulated and down-regulated genes was a $\log_2$ FC $\geq$ 2.0 and a $P \leq 0.01$.

Western blotting

The protocol of Western blotting was similar with our previous study (*65*). The brain tissue or cell sample was sonicated in radioimmunoprecipitation assay (RIPA) lysis buffer (Thermo Fisher Scientific, Rockford, IL, USA) containing protease and phosphatase inhibitors. Samples were centrifuged at 12,000*g* for 20 min at 4°C, and the protein concentrations were examined by the bicinchoninic acid assay (Beyotime Biotechnology, Haimen, China). All the protein samples were heated for 5 min at 95°C in loading buffer. The

deactivated protein samples were separated by SDS–polyacrylamide gel electrophoresis and then transferred to nitrocellulose membranes. The transferred membranes were incubated with primary antibodies and secondary antibodies. Anti-ATF6 (#ab37149; 1:500), anti–caspase 12 (ab62484; 1:1000), and anti-GRP78 (#ab21685; 1:1000) were purchased from Abcam (Cambridge, MA, USA). Anti-IRE1α (#3294; 1:500), anti-GRP78 (#3183; 1:1000), anti-HSP90α (#8165; 1:1000), and anti-HSP90β (#7411; 1:1000) were obtained from Cell Signaling Technology (San Francisco, CA, USA). Anti–p-IRE1α (#PA1-16927; 1:500) was purchased from Thermo Fisher Scientific (Waltham, MA, USA). Anti–β-actin (#sc-47778; 1:2000) was obtained from Santa Cruz Biotechnology (Waltham, MA, USA).

Biotinylation of surface proteins

Biotinylation of surface proteins was performed according to our published protocol (*66*, *67*).

For mPFC tissues

Brain slices containing mPFC region were rinsed with cold artificial cerebrospinal fluid (ACSF) containing 119.0 mM NaCl, 3.5 mM KCl, 1.3 mM $MgSO_4$, 2.5 mM $CaCl_2$, 1.0 mM NaH_2PO_4, 26.2 mM $NaHCO_3$, and 11.0 mM glucose and incubated with ACSF containing sulfo–*N*-hydroxysuccinimide (NHS)–long-chain (LC)-biotin (1 mg/ml; 21331, Thermo Fisher Scientific, Rockford, USA) for 60 min at 4°C. Unreacted biotinylation reagent was removed by quenching with cold ACSF containing 100 mM glycine for 15 min. Homogenized tissue was subsequently lysed in the RIPA buffer. Protein concentration of each lysate was quantified, and equal amounts of biotinylated proteins were then isolated using Neutravidin Agarose beads (29201, Thermo Fisher Scientific, Rockford, USA) overnight at 4°C. Biotinylated surface proteins and total proteins were measured by Western blotting.

For primary cultured cortical neuron

Briefly, primary cortical neuron cultures were washed three times with phosphate-buffered saline (PBS) (pH 7.4) and incubated with cold PBS containing sulfo-NHS-LC-biotin (1 mg/ml) for 60 min at 4°C. The reaction was terminated by quenching with cold PBS containing 200 mM glycine for 15 min at 4°C. Samples were subsequently lysed in the RIPA buffer. Protein concentration of each lysate was quantified, and equal amounts of biotinylated proteins were then isolated using Neutravidin Agarose beads overnight at 4°C.

Stereotaxic injections

For stereotaxic injection of LV or AAV, C57BL/6 mice were anesthetized with sodium pentobarbital (50 mg/kg, intraperitoneally) and placed in a stereotaxic apparatus. LV (0.8 μl) or AAV (0.3 μl) was stereotaxically delivered into the mPFC at the following coordinates: anterior-posterior, +2.0 mm; medial-lateral, ±0.4 mm; dorsal-ventral, −2.3 mm; relative to Bregma. The virus was injected with a rate of 0.05 μl/min and followed by 10 min of rest to ensure optimal virus diffusion. Lentiviral shRNAs (U6-MCS-Ubi-EGFP) directed against Gm2694 and GRP78 were obtained from GeneChem Company (Shanghai, China). The shRNA sequence–targeted Gm2694 was GGATGTTTGTCTAGAACTTAA, and the shRNA sequence–targeted GRP78 was GGGAAAGAAGGTTACCCATGC. For overexpression of Gm2694 and GRP78, AAV2/9 vector delivery system was used, and vectors carrying Gm2694 and GRP78 were constructed by AAV2/9-hSyn-Gm2694-eGFP-WPRE-SV40pA and AAV2/9-hSyn-Hspa5-eGFP-3Flag-WPRE-SV40pA, respectively.

Electrophysiological recording

Mice were anesthetized with isoflurane and then perfused with ice-cold cutting solution [210 mM sucrose, 3.1 mM sodium pyruvate, 12 mM sodium L-ascorbate, 1.0 mM NaH_2PO_4, 26.2 mM $NaHCO_3$, 5.0 mM $MgCl_2$, and 20.0 mM glucose (pH 7.2 to 7.4)]. Slices containing mPFC region were incubated in oxygenated ACSF [119.0 mM NaCl, 3.5 mM KCl, 1.3 mM $MgSO_4$, 2.5 mM $CaCl_2$, 1.0 mM NaH_2PO_4, 26.2 mM $NaHCO_3$, and 11.0 mM glucose (pH 7.2 to 7.4), 280 to 300 mOsm] for at least 1 hour at room temperature. Patch electrodes (3 to 5 megohms) were filled with internal solution [122.5 mM Cs-gluconate, 17.5 mM CsCl, 1.0 mM $MgCl_2$, 10.0 mM Hepes, 0.2 mM EGTA, 0.3 mM Na-GTP, 4.0 mM Mg-ATP, and 5 mM QX314 (pH 7.2 to 7.4), 280 to 300 mOsm]. AMPAR-mediated mEPSCs were recorded in voltage-clamp mode at a holding potential of −70 mV using Multiclamp 700B amplifier (Molecular Devices, Sunnyvale, CA, USA) in the presence of tetrodotoxin (10 μM) and bicuculline (20 μM). Data analyses were performed with pCLAMP10 software (Axon Instruments, Molecular Devices, San Jose, CA, USA).

Imaging and analysis of dendritic spine

For analysis of spine density, dendritic segments were randomly chosen from mPFC neurons that expressed GFP by injection with either target virus or scrambled virus. Dendritic segments from mPFC were imaged using a confocal laser scanning microscope (FV 1200, Olympus, Tokyo, Japan) through 60× water-immersion objective with a zoom of three, and Z-stack acquisition was performed at 0.39-μm increments. The number of spines and dendritic length were quantified by the Imaris software (Bitplane, Zurich, Switzerland). Only dendritic segments from both slices with at least 10 μm of length were included in the analysis. The spine density was presented as the number of spines per 10 μm of dendritic length.

RNA pulldown and mass spectrometry

RNA pulldown assays with biotinylated Gm2694 was performed by using a pierce magnetic RNA-protein pulldown kit (Thermo Fisher Scientific, Massachusetts, USA) according to the manufacturer's instructions. The biotin-labeled Gm2694 RNA was mixed with proteins obtained from mPFC regions of mice. The RNA binding protein complexes were purified using streptavidin agarose. The proteins were then eluted from the RNA-protein complex and detected by mass spectrometry at Shanghai Integrated Biotech Solutions Co. Ltd. (Shanghai, China) or detected by Western blotting.

Cell culture

The immortalized mouse hippocampal cell line HT22 was purchased from Guangzhou Jiniou Biotechnology Co. Ltd. (Guangzhou, Guangdong province, China). HT22 cells were cultured in Dulbecco's modified Eagle's medium (DMEM) (Gibco Laboratories, Grand Island, NY) with 10% fetal bovine serum, penicillin (100 U/ml), and streptomycin (100 μg/ml) and maintained in 5% CO_2 at 37°C.

Cultures of primary cortical neurons were prepared from postnatal day 0 (P0) to P1 C57BL/6J mice that obtained from the Animal Center of Tongji Medical College of Huazhong University of Science and Technology (HUST) (Wuhan, Hubei province, China). The isolated cortices were digested in PBS containing 0.15% trypsin (Amresco, OH, USA) at 37°C for 10 min. Cells were plated at a density of 2.5×10^5 on glass-bottom dishes coated with poly-D-lysine (500 μg/ml; BD Biosciences, NA, USA). Cells were maintained in DMEM/F12 medium (Invitrogen, Carlsbad, CA, USA) supplemented with 10%

fetal bovine serum (Invitrogen, Carlsbad, CA, USA) and 1% penicillin-streptomycin and grown in Neurobasal medium (Invitrogen, Carlsbad, CA, USA) supplemented with 2% B27 (Invitrogen, Carlsbad, CA, USA), 0.5 mM glutamine (Invitrogen, Carlsbad, CA, USA), and penicillin/streptomycin mix at 37°C and 5% CO_2. The cell culture was monitored every day for neurite outgrowth, and the cell medium was replaced with 1:1 fresh medium every 2 days. All experiments were performed on cultures from 10 to 16 days.

Primary cortical glial cells were prepared from P0 to P1 C57BL/6J mice. The isolated cortices were digested in 0.15% trypsin (Amresco, OH, USA) at 37°C for 30 min and gently triturated. Cells were plated at a density of 2.5×10^5 on glass-bottom dishes coated with poly-D-lysine (500 μg/ml; BD Biosciences, NA, USA). Cells were maintained in DMEM/F12 medium (Invitrogen, Carlsbad, CA, USA) supplemented with 10% fetal bovine serum (Invitrogen, Carlsbad, CA, USA) and 1% penicillin-streptomycin and penicillin/streptomycin mix at 37°C and 5% CO_2.

To activate UPR, primary cortical neurons were treated in the absence or presence of TM (2 μg/ml; MedChemExpress, New Jersey, USA) for 4 hours at 37°C and 95% air/5% CO_2, and then membrane protein extraction and Western blotting were performed 4 hours after transfection. LV-Gm2694 was transfected into neurons at day 8, and further experiments were carried out 7 days after transfection.

RIP analysis

RIP was performed using the Magna RIP RNA-Binding Protein Immunoprecipitation Kit (17-700, Millipore, Billerica, MA, USA) according to the manufacturer's instructions. HT22 cells were co-transfected with pcDNA3.1-GRP78 full-length and pcDNA3.1-GRP78–deleted segment vectors for 48 hours and lysed by RIPA buffer. The transfections were performed using Lipofectamine 2000 (Invitrogen, Darmstadt, Germany) according to the manufacturer's instructions. The lysate was incubated with GRP78 antibody (ab21685, Abcam, Cambridge, UK) or IgG antibody (I5006, Sigma-Aldrich, Darmstadt, Germany) for overnight at 4°C. The beads were then added and incubated for 6 hours at 4°C. The beads were washed with buffer several times and resuspended in TRIzol. The isolated RNA was transcribed to cDNA and then analyzed by qRT-PCR.

FISH and immunofluorescence

Cells grown on coverslip were fixed using 4% freshly paraformaldehyde in PBS (pH 7.4) and permeabilized by incubating with PBS containing 0.3% Triton X-100 and 5 mM vanadyl ribonucleoside complex (R3380, Sigma-Aldrich, Darmstadt, Germany) on ice for 10 min. After washing with PBS three times for 10 min each and rinsing once in 2× standard saline citrate (SSC) for 10 min, Locked Nucleic Acid (LNA) FISH probes targeting Gm2694 (TGGTACAGATGCAGAGAAGGCT) purchased from Exiqon (Exiqon A/S, Vedbaek, Denmark) and a control probe targeting S18 purchased from Guangzhou RiboBio Co. Ltd. (Guangzhou, Guangdong province, China) were added, and hybridization was performed in hybridization solution (Boster, Wuhan, Hubei province, China) for 15 hours in a humidified chamber at 40°C. After a series of wash for 30 min in 25% deionized formamide/2× SSC at 50°C, the cells on coverslips were counterstained with the primary antibody of GRP78 (ab21685, Abcam, Cambridge, UK), NeuN (ab134014, Abcam, Cambridge, UK), glial fibrillary acidic protein (3670s, Cell Signaling Technology, San Francisco, CA), Iba1 (ab5076, Abcam, Cambridge, UK), ERP72 (14712-1-AP, Proteintech, Wuhan, China), and GM130 (610822, BD Biosciences, New Jersey, USA). Secondary antibody of Alexa Fluor 488 (Invitrogen, Carlsbad, CA) and Alexa Fluor 647 (Invitrogen, Carlsbad, CA) were counterstained with 4′,6-diamidino-2phenylindole (DAPI) and then imaged using a confocal microscope (FV1200, Olympus, Tokyo, Japan).

Fluorescence resonance energy transfer

HT22 cells were fixed with 4% paraformaldehyde in PBS and permeabilized with 0.3% Triton X-100. After washing with PBS three times for 10 min each and rinsed once in 2× SSC for 10 min, cells were incubated with Gm2694 probe (Exiqon, Vedbaek, Denmark) in a humidified chamber overnight at 40°C. The cells were washed with SSC on the next day and incubated with primary antibody of GRP78 (ab21685, Abcam, Cambridge, UK) overnight at 4°C. On the 3rd day, cells were washed with PBS and incubated with secondary Alexa Fluor 647–labeled antibody (A-31573, Invitrogen, Carlsbad, CA) at room temperature for 2 hours in the dark. After washing several times by PBS, cells were mounted with Vectashield (Vector Laboratories, Burlingame, CA), and FRET analysis was performed using a confocal microscope (FV1200, Olympus, Tokyo, Japan). The data of confocal FRET microscopy were obtained from at least three different experiments as described previously (*68*). Images were acquired with 60×/1.42 of numerical aperture oil objective and analyzed with FluoView software using the sensitized emission method. FRET efficiency and distance were calculated by selecting regions of interest.

Statistical analysis

Animals were randomly assigned to experimental groups. Data are given as means ± SEM and obtained from the number of separate experiments indicated. Comparison between two groups was evaluated by unpaired Student's *t* test. Differences in different treatment groups were carried out using one-way or two-way analysis of variance (ANOVA), followed by Bonferroni's post hoc multiple comparison tests. Data were analyzed using GraphPad Prism 8.0 (GraphPad software, CA, USA), and statistical significance was defined as $P < 0.05$.

SUPPLEMENTARY MATERIALS

Supplementary material for this article is available at https://science.org/doi/10.1126/sciadv.abn2496

View/request a protocol for this paper from *Bio-protocol*.

REFERENCES AND NOTES

1. O. Berton, E. J. Nestler, New approaches to antidepressant drug discovery: Beyond monoamines. *Nat. Rev. Neurosci.* **7**, 137–151 (2006).
2. H. K. Manji, W. C. Drevets, D. S. Charney, The cellular neurobiology of depression. *Nat. Med.* **7**, 541–547 (2001).
3. J. Savitz, W. C. Drevets, Bipolar and major depressive disorder: Neuroimaging the developmental-degenerative divide. *Neurosci. Biobehav. Rev.* **33**, 699–771 (2009).
4. H. J. Kang, B. Voleti, T. Hajszan, G. Rajkowska, C. A. Stockmeier, P. Licznerski, A. Lepack, M. S. Majik, L. S. Jeong, M. Banasr, H. Son, R. S. Duman, Decreased expression of synapse-related genes and loss of synapses in major depressive disorder. *Nat. Med.* **18**, 1413–1417 (2012).
5. R. S. Duman, G. K. Aghajanian, Synaptic dysfunction in depression: Potential therapeutic targets. *Science* **338**, 68–72 (2012).
6. J. L. Rinn, H. Y. Chang, Genome regulation by long noncoding RNAs. *Annu. Rev. Biochem.* **81**, 145–166 (2012).
7. K. C. Wang, H. Y. Chang, Molecular mechanisms of long noncoding RNAs. *Mol. Cell* **43**, 904–914 (2011).
8. J. A. Briggs, E. J. Wolvetang, J. S. Mattick, J. L. Rinn, G. Barry, Mechanisms of long non-coding RNAs in mammalian nervous system development, plasticity, disease, and evolution. *Neuron* **88**, 861–877 (2015).
9. E. Grinman, Y. Nakahata, Y. Avchalumov, I. Espadas, S. Swarnkar, R. Yasuda, S. V. Puthanveettil, Activity-regulated synaptic targeting of lncRNA ADEPTR mediates

structural plasticity by localizing Sptn1 and AnkB in dendrites. *Sci. Adv.* **7**, eabf0605 (2021).
10. D. Bernard, K. V. Prasanth, V. Tripathi, S. Colasse, T. Nakamura, Z. Xuan, M. Q. Zhang, F. Sedel, L. Jourdren, F. Coulpier, A. Triller, D. L. Spector, A. Bessis, A long nuclear-retained non-coding RNA regulates synaptogenesis by modulating gene expression. *EMBO J.* **29**, 3082–3093 (2010).
11. P. J. Ross, W. B. Zhang, R. S. F. Mok, K. Zaslavsky, E. Deneault, L. D'Abate, D. C. Rodrigues, R. K. C. Yuen, M. Faheem, M. Mufteev, A. Piekna, W. Wei, P. Pasceri, R. J. Landa, A. Nagy, B. Varga, M. W. Salter, S. W. Scherer, J. Ellis, Synaptic dysfunction in human neurons with autism-associated deletions in PTCHD1-AS. *Biol. Psychiatry* **87**, 139–149 (2020).
12. B. L. Raveendra, S. Swarnkar, Y. Avchalumov, X. A. Liu, E. Grinman, K. Badal, A. Reich, B. D. Pascal, S. V. Puthanveettil, Long noncoding RNA GM12371 acts as a transcriptional regulator of synapse function. *Proc. Natl. Acad. Sci. U.S.A.* **115**, E10197–E10205 (2018).
13. N. N. Parikshak, V. Swarup, T. G. Belgard, M. Irimia, G. Ramaswami, M. J. Gandal, C. Hartl, V. Leppa, L. T. Ubieta, J. Huang, J. K. Lowe, B. J. Blencowe, S. Horvath, D. H. Geschwind, Genome-wide changes in lncRNA, splicing, and regional gene expression patterns in autism. *Nature* **540**, 423–427 (2016).
14. L. Meng, A. J. Ward, S. Chun, C. F. Bennett, A. L. Beaudet, F. Rigo, Towards a therapy for Angelman syndrome by targeting a long non-coding RNA. *Nature* **518**, 409–412 (2015).
15. M. A. Faghihi, F. Modarresi, A. M. Khalil, D. E. Wood, B. G. Sahagan, T. E. Morgan, C. E. Finch, G. St. Laurent III, P. J. Kenny, C. Wahlestedt, Expression of a noncoding RNA is elevated in Alzheimer's disease and drives rapid feed-forward regulation of beta-secretase. *Nat. Med.* **14**, 723–730 (2008).
16. H. Xu, A. N. Brown, N. J. Waddell, X. Liu, G. J. Kaplan, J. M. Chitaman, V. Stockman, R. L. Hedinger, R. Adams, K. Abreu, L. Shen, R. Neve, Z. Wang, E. J. Nestler, J. Feng, Role of long noncoding RNA Gas5 in cocaine action. *Biol. Psychiatry* **88**, 758–766 (2020).
17. G. Barry, J. A. Briggs, D. P. Vanichkina, E. M. Poth, N. J. Beveridge, V. S. Ratnu, S. P. Nayler, K. Nones, J. Hu, T. W. Bredy, S. Nakagawa, F. Rigo, R. J. Taft, M. J. Cairns, S. Blackshaw, E. J. Wolvetang, J. S. Mattick, The long non-coding RNA Gomafu is acutely regulated in response to neuronal activation and involved in schizophrenia-associated alternative splicing. *Mol. Psychiatry* **19**, 486–494 (2014).
18. B. Labonte, O. Engmann, I. Purushothaman, C. Menard, J. Wang, C. Tan, J. R. Scarpa, G. Moy, Y. E. Loh, M. Cahill, Z. S. Lorsch, P. J. Hamilton, E. S. Calipari, G. E. Hodes, O. Issler, H. Kronman, M. Pfau, A. L. J. Obradovic, Y. Dong, R. L. Neve, S. Russo, A. Kazarskis, C. Tamminga, N. Mechawar, G. Turecki, B. Zhang, L. Shen, E. J. Nestler, Sex-specific transcriptional signatures in human depression. *Nat. Med.* **23**, 1102–1111 (2017).
19. O. Issler, Y. Y. van der Zee, A. Ramakrishnan, J. Wang, C. Tan, Y. E. Loh, I. Purushothaman, D. M. Walker, Z. S. Lorsch, P. J. Hamilton, C. J. Pena, E. Flaherty, B. J. Hartley, A. Torres-Berrio, E. M. Parise, H. Kronman, J. E. Duffy, M. S. Estill, E. S. Calipari, B. Labonte, R. L. Neve, C. A. Tamminga, K. J. Brennand, Y. Dong, L. Shen, E. J. Nestler, Sex-specific role for the long non-coding RNA LINC00473 in depression. *Neuron* **106**, 912–926.e5 (2020).
20. M. X. Li, H. L. Zheng, Y. Luo, J. G. He, W. Wang, J. Han, L. Zhang, X. Wang, L. Ni, H. Y. Zhou, Z. L. Hu, P. F. Wu, Y. Jin, L. H. Long, H. Zhang, G. Hu, J. G. Chen, F. Wang, Gene deficiency and pharmacological inhibition of caspase-1 confers resilience to chronic social defeat stress via regulating the stability of surface AMPARs. *Mol. Psychiatry* **23**, 556–568 (2018).
21. D. Lv, Y. Chen, M. Shen, X. Liu, Y. Zhang, J. Xu, C. Wang, Mechanisms underlying the rapid-acting antidepressant-like effects of neuropeptide VGF (non-acronymic) C-terminal peptide TLQP-62. *Neuropharmacology* **143**, 317–326 (2018).
22. R. X. Zhang, Y. Han, C. Chen, L. Z. Xu, J. L. Li, N. Chen, C. Y. Sun, W. H. Chen, W. L. Zhu, J. Shi, L. Lu, EphB2 in the medial prefrontal cortex regulates vulnerability to stress. *Neuropsychopharmacology* **41**, 2541–2556 (2016).
23. J. Schwenk, S. Boudkkazi, M. K. Kocylowski, A. Brechet, G. Zolles, T. Bus, K. Costa, A. Kollewe, J. Jordan, J. Bank, W. Bildl, R. Sprengel, A. Kulik, J. Roeper, U. Schulte, B. Fakler, An ER assembly line of AMPA-receptors controls excitatory neurotransmission and its plasticity. *Neuron* **104**, 680–692.e9 (2019).
24. W. Vandenberghe, R. A. Nicoll, D. S. Bredt, Interaction with the unfolded protein response reveals a role for stargazin in biosynthetic AMPA receptor transport. *J. Neurosci.* **25**, 1095–1102 (2005).
25. J. Liu, Y. Wang, L. Song, L. Zeng, W. Yi, T. Liu, H. Chen, M. Wang, Z. Ju, Y. S. Cong, A critical role of DDRGK1 in endoplasmic reticulum homoeostasis via regulation of IRE1α stability. *Nat. Commun.* **8**, 14186 (2017).
26. M. Schroder, R. J. Kaufman, The mammalian unfolded protein response. *Annu. Rev. Biochem.* **74**, 739–789 (2005).
27. X. M. Zhang, X. Y. Yan, B. Zhang, Q. Yang, M. Ye, W. Cao, W. B. Qiang, L. J. Zhu, Y. L. Du, X. X. Xu, J. S. Wang, F. Xu, W. Lu, S. Qiu, W. Yang, J. H. Luo, Activity-induced synaptic delivery of the GluN2A-containing NMDA receptor is dependent on endoplasmic reticulum chaperone Bip and involved in fear memory. *Cell Res.* **25**, 818–836 (2015).
28. I. H. Greger, L. Khatri, E. B. Ziff, RNA editing at arg607 controls AMPA receptor exit from the endoplasmic reticulum. *Neuron* **34**, 759–772 (2002).
29. M. E. Rubio, R. J. Wenthold, Differential distribution of intracellular glutamate receptors in dendrites. *J. Neurosci.* **19**, 5549–5562 (1999).
30. M. E. Rubio, R. J. Wenthold, Calnexin and the immunoglobulin binding protein (BiP) coimmunoprecipitate with AMPA receptors. *J. Neurochem.* **73**, 942–948 (1999).
31. C. Bown, J. F. Wang, G. MacQueen, L. T. Young, Increased temporal cortex ER stress proteins in depressed subjects who died by suicide. *Neuropsychopharmacology* **22**, 327–332 (2000).
32. Y. Yoshino, Y. Dwivedi, Elevated expression of unfolded protein response genes in the prefrontal cortex of depressed subjects: Effect of suicide. *J. Affect. Disord.* **262**, 229–236 (2020).
33. F. C. Bischoff, A. Werner, D. John, J. N. Boeckel, M. T. Melissari, P. Grote, S. F. Glaser, S. Demolli, S. Uchida, K. M. Michalik, B. Meder, H. A. Katus, J. Haas, W. Chen, S. S. Pullamsetti, W. Seeger, A. M. Zeiher, S. Dimmeler, C. M. Zehendner, Identification and functional characterization of hypoxia-induced endoplasmic reticulum stress regulating lncRNA (HypERlnc) in pericytes. *Circ. Res.* **121**, 368–375 (2017).
34. M. Kato, M. Wang, Z. Chen, K. Bhatt, H. J. Oh, L. Lanting, S. Deshpande, Y. Jia, J. Y. Lai, C. L. O'Connor, Y. Wu, J. B. Hodgin, R. G. Nelson, M. Bitzer, R. Natarajan, An endoplasmic reticulum stress-regulated lncRNA hosting a microRNA megacluster induces early features of diabetic nephropathy. *Nat. Commun.* **7**, 12864 (2016).
35. Z. F. Deng, H. L. Zheng, J. G. Chen, Y. Luo, J. F. Xu, G. Zhao, J. J. Lu, H. H. Li, S. Q. Gao, D. Z. Zhang, L. Q. Zhu, Y. H. Zhang, F. Wang, miR-214-3p Targets β-catenin to regulate depressive-like behaviors induced by chronic social defeat stress in mice. *Cereb. Cortex* **29**, 1509–1519 (2019).
36. L. Statello, C. J. Guo, L. L. Chen, M. Huarte, Gene regulation by long non-coding RNAs and its biological functions. *Nat. Rev. Mol. Cell Biol.* **22**, 96–118 (2021).
37. J. W. Murrough, C. G. Abdallah, S. J. Mathew, Targeting glutamate signalling in depression: Progress and prospects. *Nat. Rev. Drug Discov.* **16**, 472–486 (2017).
38. C. Menard, M. L. Pfau, G. E. Hodes, V. Kana, V. X. Wang, S. Bouchard, A. Takahashi, M. E. Flanigan, H. Aleyasin, K. B. LeClair, W. G. Janssen, B. Labonte, E. M. Parise, Z. S. Lorsch, S. A. Golden, M. Heshmati, C. Tamminga, G. Turecki, M. Campbell, Z. A. Fayad, C. Y. Tang, M. Merad, S. J. Russo, Social stress induces neurovascular pathology promoting depression. *Nat. Neurosci.* **20**, 1752–1760 (2017).
39. D. M. Ribeiro, A. Zanzoni, A. Cipriano, R. Delli Ponti, L. Spinelli, M. Ballarino, I. Bozzoni, G. G. Tartaglia, C. Brun, Protein complex scaffolding predicted as a prevalent function of long non-coding RNAs. *Nucleic Acids Res.* **46**, 917–928 (2018).
40. X. Z. Wang, H. P. Harding, Y. Zhang, E. M. Jolicoeur, M. Kuroda, D. Ron, Cloning of mammalian Ire1 reveals diversity in the ER stress responses. *EMBO J.* **17**, 5708–5717 (1998).
41. J. J. Martindale, R. Fernandez, D. Thuerauf, R. Whittaker, N. Gude, M. A. Sussman, C. C. Glembotski, Endoplasmic reticulum stress gene induction and protection from ischemia/reperfusion injury in the hearts of transgenic mice with a tamoxifen-regulated form of ATF6. *Circ. Res.* **98**, 1186–1193 (2006).
42. Y. Fukata, A. V. Tzingounis, J. C. Trinidad, M. Fukata, A. L. Burlingame, R. A. Nicoll, D. S. Bredt, Molecular constituents of neuronal AMPA receptors. *J. Cell Biol.* **169**, 399–404 (2005).
43. A. Torres-Berrio, D. Nouel, S. Cuesta, E. M. Parise, J. M. Restrepo-Lozano, P. Larochelle, E. J. Nestler, C. Flores, MiR-218: A molecular switch and potential biomarker of susceptibility to stress. *Mol. Psychiatry* **25**, 951–964 (2019).
44. Y. Zhang, L. Du, Y. Bai, B. Han, C. He, L. Gong, R. Huang, L. Shen, J. Chao, P. Liu, H. Zhang, H. Zhang, L. Gu, J. Li, G. Hu, C. Xie, Z. Zhang, H. Yao, CircDYM ameliorates depressive-like behavior by targeting miR-9 to regulate microglial activation via HSP90 ubiquitination. *Mol. Psychiatry* **25**, 1175–1190 (2018).
45. R. Huang, Y. Zhang, Y. Bai, B. Han, M. Ju, B. Chen, L. Yang, Y. Wang, H. Zhang, H. Zhang, C. Xie, Z. Zhang, H. Yao, N^6-methyladenosine modification of fatty acid amide hydrolase messenger RNA in circular RNA STAG1-regulated astrocyte dysfunction and depressive-like behaviors. *Biol. Psychiatry* **88**, 392–404 (2020).
46. S. A. Golden, D. J. Christoffel, M. Heshmati, G. E. Hodes, J. Magida, K. Davis, M. E. Cahill, C. Dias, E. Ribeiro, J. L. Ables, P. J. Kennedy, A. J. Robison, J. Gonzalez-Maeso, R. L. Neve, G. Turecki, S. Ghose, C. A. Tamminga, S. J. Russo, Epigenetic regulation of RAC1 induces synaptic remodeling in stress disorders and depression. *Nat. Med.* **19**, 337–344 (2013).
47. S. S. Hwang, J. Lim, Z. Yu, P. Kong, E. Sefik, H. Xu, C. C. D. Harman, L. K. Kim, G. R. Lee, H. B. Li, R. A. Flavell, mRNA destabilization by BTG1 and BTG2 maintains T cell quiescence. *Science* **367**, 1255–1260 (2020).
48. Y. Zhang, X. Zhang, B. Cai, Y. Li, Y. Jiang, X. Fu, Y. Zhao, H. Gao, Y. Yang, J. Yang, S. Li, H. Wu, X. Jin, G. Xue, J. Yang, W. Ma, Q. Han, T. Tian, Y. Li, B. Yang, Y. Lu, Z. Pan, The long noncoding RNA lncCIRBIL disrupts the nuclear translocation of Bclaf1 alleviating cardiac ischemia-reperfusion injury. *Nat. Commun.* **12**, 522 (2021).
49. M. M. Lou, X. Q. Tang, G. M. Wang, J. He, F. Luo, M. F. Guan, F. Wang, H. Zou, J. Y. Wang, Q. Zhang, M. J. Xu, Q. L. Shi, L. B. Shen, G. M. Ma, Y. Wu, Y. Y. Zhang, A. B. Liang, T. H. Wang, L. L. Xiong, J. Wang, J. Xu, W. Y. Wang, Long noncoding RNA BS-DRL1 modulates the DNA damage response and genome stability by interacting with HMGB1 in neurons. *Nat. Commun.* **12**, 4075 (2021).

50. D. He, J. Wang, Y. Lu, Y. Deng, C. Zhao, L. Xu, Y. Chen, Y. C. Hu, W. Zhou, Q. R. Lu, lncRNA functional networks in oligodendrocytes reveal stage-specific myelination control by an lncOL1/Suz12 complex in the CNS. *Neuron* **93**, 362–378 (2017).
51. Y. P. Li, F. F. Duan, Y. T. Zhao, K. L. Gu, L. Q. Liao, H. B. Su, J. Hao, K. Zhang, N. Yang, Y. Wang, A TRIM71 binding long noncoding RNA Trincr1 represses FGF/ERK signaling in embryonic stem cells. *Nat. Commun.* **10**, 1368 (2019).
52. Y. Jin, B. Zhang, J. Lu, Y. Song, W. Wang, W. Zhang, F. Shao, M. Gong, M. Wang, X. Liang, S. Li, Z. Zhang, G. Shan, X. Wang, Long noncoding RNA PM maintains cerebellar synaptic integrity and Cbln1 activation via Pax6/Mll1-mediated H3K4me3. *PLOS Biol.* **19**, e3001297 (2021).
53. C. Wang, Y. Li, S. Yan, H. Wang, X. Shao, M. Xiao, B. Yang, G. Qin, R. Kong, R. Chen, N. Zhang, Interactome analysis reveals that lncRNA HULC promotes aerobic glycolysis through LDHA and PKM2. *Nat. Commun.* **11**, 3162 (2020).
54. C. Casas, GRP78 at the centre of the stage in cancer and neuroprotection. *Front. Neurosci.* **11**, 177 (2017).
55. Y. W. Liu, R. Xia, K. Lu, M. Xie, F. Yang, M. Sun, W. De, C. Wang, G. Ji, LincRNAFEZF1-AS1 represses p21 expression to promote gastric cancer proliferation through LSD1-mediated H3K4me2 demethylation. *Mol. Cancer* **16**, 39 (2017).
56. X. Wei, A. S. Howell, X. Dong, C. A. Taylor, R. C. Cooper, J. Zhang, W. Zou, D. R. Sherwood, K. Shen, The unfolded protein response is required for dendrite morphogenesis. *eLife* **4**, e06963 (2015).
57. L. Wen, F. Han, Y. Shi, X. Li, Role of the endoplasmic reticulum pathway in the medial prefrontal cortex in post-traumatic stress disorder model rats. *J. Mol. Neurosci.* **59**, 471–482 (2016).
58. S. L. Gourley, F. J. Wu, D. D. Kiraly, J. E. Ploski, A. T. Kedves, R. S. Duman, J. R. Taylor, Regionally specific regulation of ERK MAP kinase in a model of antidepressant-sensitive chronic depression. *Biol. Psychiatry* **63**, 353–359 (2008).
59. J. Shim, T. Umemura, E. Nothstein, C. Rongo, The unfolded protein response regulates glutamate receptor export from the endoplasmic reticulum. *Mol. Biol. Cell* **15**, 4818–4828 (2004).
60. M. Kuijpers, G. Kochlamazashvili, A. Stumpf, D. Puchkov, A. Swaminathan, M. T. Lucht, E. Krause, T. Maritzen, D. Schmitz, V. Haucke, Neuronal autophagy regulates presynaptic neurotransmission by controlling the axonal endoplasmic reticulum. *Neuron* **109**, 299–313.e9 (2020).
61. T. Zhao, J. Du, H. Zeng, Interplay between endoplasmic reticulum stress and non-coding RNAs in cancer. *J. Hematol. Oncol.* **13**, 163 (2020).
62. S. Keihani, V. Kluever, S. Mandad, V. Bansal, R. Rahman, E. Fritsch, L. C. Gomes, A. Gartner, S. Kugler, H. Urlaub, J. D. Wren, S. Bonn, S. O. Rizzoli, E. F. Fornasiero, The long noncoding RNA neuroLNC regulates presynaptic activity by interacting with the neurodegeneration-associated protein TDP-43. *Sci. Adv.* **5**, eaay2670 (2019).
63. M. Ma, W. Xiong, F. Hu, M. F. Deng, X. Huang, J. G. Chen, H. Y. Man, Y. Lu, D. Liu, L. Q. Zhu, A novel pathway regulates social hierarchy via lncRNA AtLAS and postsynaptic synapsin IIb. *Cell Res.* **30**, 105–118 (2020).
64. J. G. He, H. Y. Zhou, S. G. Xue, J. J. Lu, J. F. Xu, B. Zhou, Z. L. Hu, P. F. Wu, L. H. Long, L. Ni, Y. Jin, F. Wang, J. G. Chen, Transcription factor TWIST1 integrates dendritic remodeling and chronic stress to promote depressive-like behaviors. *Biol. Psychiatry* **89**, 615–626 (2020).
65. H. Y. Zhou, J. G. He, Z. L. Hu, S. G. Xue, J. F. Xu, Q. Q. Cui, S. Q. Gao, B. Zhou, P. F. Wu, L. H. Long, F. Wang, J. G. Chen, A-kinase anchoring protein 150 and protein kinase A complex in the basolateral amygdala contributes to depressive-like behaviors induced by chronic restraint stress. *Biol. Psychiatry* **86**, 131–142 (2019).
66. K. Li, H. S. Chen, D. Li, H. H. Li, J. Wang, L. Jia, P. F. Wu, L. H. Long, Z. L. Hu, J. G. Chen, F. Wang, SAR405, a highly specific VPS34 inhibitor, disrupts auditory fear memory consolidation of mice via facilitation of inhibitory neurotransmission in basolateral amygdala. *Biol. Psychiatry* **85**, 214–225 (2019).
67. J. Fan, D. Li, H. S. Chen, J. G. Huang, J. F. Xu, W. W. Zhu, J. G. Chen, F. Wang, Metformin produces anxiolytic-like effects in rats by facilitating GABAA receptor trafficking to membrane. *Br. J. Pharmacol.* **176**, 297–316 (2019).
68. A. Kern, M. Mavrikaki, C. Ullrich, R. Albarran-Zeckler, A. F. Brantley, R. G. Smith, Hippocampal dopamine/DRD1 signaling dependent on the ghrelin receptor. *Cell* **163**, 1176–1190 (2015).

Acknowledgments

Funding: This work was supported by the Foundation for National Key R&D Program of China (no. 2021ZD0202900 to J.G.C.), National Natural Science Foundation of China (nos. 82130110 to J.G.C., U21A20363 to F.W., 81721005 to J.G.C. and F.W., and 81903593 to H.-S.C.), Chinese Postdoctoral Science Foundation Funded Project (no. 2019M652657 to H.-S.C.), and Program for Changjiang Scholars and Innovative Research Team in University (no. IRT13016 to J.G.C.).
Author contributions: H.-S.C. designed and performed most experiments, analyzed the data, and wrote the manuscript. X.W., R.-S.Z., and R.Z. performed the quantitative PCR and participated the behavioral tests and analysis. J.W. performed the immunofluorescence and analysis of dendrite spine. H.-H.L. performed the virus injection. T.D. performed the Western blotting. Y.-K.L. cultured the primary cortical neurons and the HT22 cells. W.-L.X. helped to draw the figure of mechanism. G.Z. designed experiments and analyzed the data. J.-G.C. and F.W. supervised the project, designed experiments, and supported funding acquisition. J.W., S.-Q.Z. and H.-J.W. performed the immunofluorescence and analysis of dendrite spine.
Competing interests: The authors declare that they have no competing interests. **Data and materials availability:** All data needed to evaluate the conclusions in the paper are present in the paper and/or the Supplementary Materials.

Submitted 14 November 2021
Accepted 18 October 2022
Published 2 December 2022
10.1126/sciadv.abn2496